Dynamics of waves in one-dimensional electron systems: Density oscillations driven by population inversion

I. V. Protopopov,[1,2] D. B. Gutman,[1,3] P. Schmitteckert,[1,4] and A. D. Mirlin[1,4,5,6]

[1]*Institut für Nanotechnologie, Karlsruhe Institute of Technology, 76021 Karlsruhe, Germany*

[2]*L. D. Landau Institute for Theoretical Physics RAS, 119334 Moscow, Russia*

[3]*Department of Physics, Bar Ilan University, Ramat Gan 52900, Israel*

[4]*DFG Center for Functional Nanostructures, Karlsruhe Institute of Technology, 76128 Karlsruhe, Germany*

[5]*Institut für Theorie der kondensierten Materie, Karlsruhe Institute of Technology, 76128 Karlsruhe, Germany*

[6]*Petersburg Nuclear Physics Institute, 188300 St. Petersburg, Russia*

(Received 5 September 2012; revised manuscript received 11 December 2012; published 14 January 2013)

We explore dynamics of a density pulse induced by a local quench in a one-dimensional electron system. The spectral curvature leads to an "overturn" (population inversion) of the wave. We show that beyond this time, the density profile develops strong oscillations with a period much larger than the Fermi wavelength. The effect is studied first for the case of free fermions by means of direct quantum simulations and via semiclassical analysis of the evolution of Wigner function. We demonstrate then that the period of oscillations is correctly reproduced by a hydrodynamic theory with an appropriate dispersive term. Finally, we explore the effect of different types of electron-electron interaction on the phenomenon. We show that sufficiently strong interaction [$U(r) \gg 1/mr^2$ where m is the fermionic mass and r the relevant spatial scale] determines the dominant dispersive term in the hydrodynamic equations. Hydrodynamic theory reveals crucial dependence of the density evolution on the relative sign of the interaction and the density perturbation.

DOI: 10.1103/PhysRevB.87.045112 PACS number(s): 73.23.−b, 73.21.Hb, 71.10.Pm

I. INTRODUCTION

Transport properties of interacting one-dimensional (1D) systems keep attracting a great deal of research interest. Experimental realizations of 1D fermionic systems include, in particular, carbon nanotubes, semiconductor and metallic nanowires, as well as quantum Hall (and other topological insulator) edges. Further, 1D bosonic and fermionic systems can be engineered by using cold atomic gases in optical traps of the corresponding geometry. A standard and powerful theoretical approach to interacting 1D systems is the bosonization.[1–5] When (i) the spectrum is linearized, (ii) backscattering processes are neglected, and (iii) the physics near equilibrium is explored, the bosonization reduces the original interacting problem to a Gaussian field theory, thus reducing evaluation of physical observables to a straightforward calculation of Gaussian integrals. When one (or several) of the above three conditions is not fulfilled, the theoretical analysis becomes much more involved. In this paper, we will focus on nonequilibrium physics of 1D fermionic systems in the regime where the spectral curvature is of crucial importance.

Properties of 1D interacting systems with spectral nonlinearity have been addressed in a series of recent theoretical works.[6–10] Here, we will consider the time evolution of a density pulse created by a local quench in a 1D fermionic system (that will be assumed to be spinless or spin polarized for simplicity). We will assume that this pulse is quasiclassical (i.e., has a characteristic spatial extension much larger than the Fermi wavelength) and sufficiently strong (i.e., contains a large number of electrons). For not too long times, the evolution seems to be fully harmless: the pulse splits into left- and right-moving parts that separate and move away from each other, approximately preserving their shape. The key point is that the shape would remain strictly unchanged only for linear dispersion of excitations, while the nonlinearity of dispersion leads to a deformation of the pulse. As a result, at a certain finite time, the pulse tends to "overturn." The problem to be addressed is what happens with the density profile beyond this time.

The above problem was formulated in Ref. 11 in the context of the Calogero model that was argued to describe the fractional quantum Hall (FQH) edges (see also a recent paper, Ref. 12). Using a quantum hydrodynamics approach, the authors of Refs. 11 and 12 came to a conclusion that a density pulse formed in a FQH edge will evolve in a sequence of well-separated solitons with a quantized charge (equal to ν for Laughlin states).

In this work, we perform a systematic analysis of the pulse dynamics for free fermions as well for those with different types of interaction. We begin by considering a noninteracting case (Sec. II). Quantum simulations show development of density oscillations at sufficiently large times. By analyzing evolution of the Wigner function, we show that once the semiclassical phase-space distribution overturns (i.e., develops a population inversion characterized by three "Fermi momenta"), strong oscillations of density are generated in the corresponding region of space. The characteristic scale of these oscillations is much larger than the Fermi wavelength λ_F. The oscillations can be understood as Friedel oscillations between different Fermi-momentum branches.

In Sec. III, we switch to the bosonization language and discuss a connection between free-fermion oscillations studied in Sec. II and classical hydrodynamics. In the latter class of problems,[13] oscillating structures are known to develop when shock waves are regularized by dispersive terms. We show that although dispersive terms arise already within Haldane bosonization formalism of free fermions with curvature, the dominant terms should come from summing the loop

expansion. While we do not know how to take into account these effects systematically, we approximate them by including in the classical hydrodynamic equation a term corresponding to an upper (for a positive pulse) branch of the particle-hole continuum. Solving the corresponding equation (which is of Benjamin-Ono type), we show that it yields oscillations with correct period (including its spatial variation) but with an amplitude several times larger than the correct one. This shows that the above classical hydrodynamic equation does catch some important physics of the developing "dispersive shock" of a free-fermion pulse but does not represent a fully controllable approximation.

Section IV is devoted to an analysis of the interaction effects on the pulse evolution. We consider first the case of a short-range interaction and argue that the discovered oscillations remain largely preserved, up to two modifications: (i) conventional Luttinger-liquid renormalization of the Fermi velocity, and (ii) washing out of oscillations at long times due to inelastic processes. We turn then to the case of a long-range interaction. We show that when the interaction decays sufficiently slowly (specifically, $U(r) \gg 1/mr^2$ at large distances r, and m is an electronic mass), the leading contribution to the dispersion results from the interaction term, and the problem can be treated quasiclassically (i.e., loops can be neglected), giving rise to a classical hydrodynamic equation. The evolution of the pulse according to such an equation depends crucially on the sign of the pulse and the sign of the interaction (or, more precisely, on the relative sign between them). When the interaction is repulsive and the density pulse is downward, oscillations develop similarly to the case of free fermions (or short-range interaction). The period of oscillations gets, however, parametrically larger. On the other hand, for an upward pulse (and still assuming a repulsive long-range interaction), the pulse splits in a sequence of "solitons" (whose charge is in general not quantized, except for the case of $1/r^2$ interaction). Section V contains a summary of our results and a discussion of prospective research directions.

II. FREE FERMIONS

In this section and in Sec. III, we study the evolution of a "quasiclassical" density disturbance of the Fermi sea of free fermions. We begin (Sec. II A) by formulating the problem and performing its numerical modeling, which shows emergence of density oscillations after the time corresponding to overturning of the initial packet. In Sec. II B, we solve this problem analytically by using the straightforward ("fermionic") approach. Specifically, we demonstrate that, once the dispersion induces a population inversion within the pulse, phase-space oscillation of the Wigner function gives rise to density oscillations. Analyzing the resulting density oscillations, we find a perfect agreement with the results of numerical simulations of Sec. II A. Finally, in Sec. III, we make a link to "dispersive shocks" in the classical hydrodynamics. We show that when the dispersive term corresponding to the appropriate branch of the particle-hole spectrum is incorporated into classical hydrodynamic equations, the latter reproduce correctly the period of emerging oscillations (but considerably overestimate their amplitude).

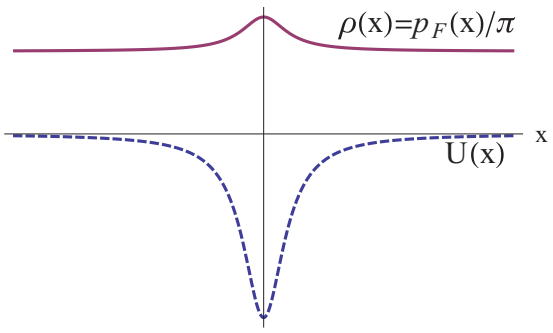

FIG. 1. (Color online) Setup. Density disturbance in the Fermi sea is created by the application of a potential $U(x)$ which is then switched off at $t = 0$.

A. Formulation of the problem and numerical simulations

The problem that we address is formulated in a rather simple way. We assume that a nonuniform fermionic density was created by application of a smooth (on the scale of λ_F) and relatively weak (compared to the Fermi energy ϵ_F) external potential $U(x)$ to the unperturbed Fermi sea (Fig. 1). The system at $t < 0$ is in its ground state characterized by the fermionic density

$$\rho_0(x) \equiv \frac{p_F(x)}{\pi} = \frac{1}{\pi}\sqrt{p_\infty^2 - 2mU(x)}\,. \tag{1}$$

Here, p_∞ is the Fermi momentum at infinity. Note that all the corrections to the semiclassical result (1) are exponentially small as long as $U(x)$ is smooth on the scale of λ_F. For transparency of discussion, we assume that the density pulse has a shape of a single hump (as shown schematically in Fig. 1), i.e., that $U(x) < 0$ and has a single minimum at $x = 0$.

At $t = 0$, the potential is suddenly switched off, which results in the appearance of a nonequilibrium state and subsequent propagation of the density perturbation created by $U(x)$. Our goal will be to explore this density evolution at sufficiently long times. We will assume that the number of particles within the initial pulse is large, $\Delta x\, \Delta\rho \gg 1$, where Δx and $\Delta\rho$ are the characteristic extension of the pulse and its amplitude, respectively. The interesting physics will emerge at times $t > t_c \sim m\Delta x/\Delta\rho$, when the semiclassical phase-space distribution overturns.

Since the fermions are free and their state was prepared in the coherent manner described above, the full information on the quantum state of the system is encoded in the Wigner function

$$f(X,p;t) = \int dy\, e^{-ipy}\langle\psi^+(X_-;t)\psi(X_+;t)\rangle,$$
$$X_\pm = X \pm \frac{y}{2} \tag{2}$$

satisfying at $t > 0$ the (exact!) Boltzmann equation

$$\partial_t f(X,p;t) + p\partial_X f(X,p;t) = 0. \tag{3}$$

In this equation, we have set the particle mass to unity. Let us note that the mass m will enter our results only through the overall time scale. Thus, dependence on m can be eliminated completely by measuring t in units of t_c.

Equation (3) is trivially solved, yielding

$$f(X,p;t) = f\,(X - pt, p; t = 0) \equiv f_0\,(X - pt, p)\,. \quad (4)$$

Therefore, once we know the Wigner function of the initial ($t = 0$) state, the Wigner function of the evolved ($t > 0$) state can be immediately obtained.

Let us examine now the Wigner function of the initial state. Semiclassically, one would expect that $f_0(X,p)$ takes value unity for the occupied electronic states that are below the position-dependent Fermi momentum $p_F(X)$ and is zero for empty ones [above $p_F(X)$]:

$$f_0(X,p) = \Theta\big[p_F^2(X) - p^2\big]. \quad (5)$$

In this approximation, the time-dependent state of the fermions after the quench (i.e., at $t > 0$) is fully characterized by the Fermi surface $p_F(x,t)$ separating occupied and unoccupied single-particle states in the phase space and satisfying the Euler equation [we concentrate on the Fermi surface for the right-moving particles with $p_F(x) > 0$]

$$\partial_t p_F(x,t) + p_F(x,t)\partial_x p_F(x,t) = 0. \quad (6)$$

While capturing correctly the physics at small times, the Euler equation (6) suffers from the shock-wave phenomenon. Specifically, for arbitrarily smooth initial conditions, the curvature of the electronic dispersion relation $\epsilon(p) = p^2/2$ makes the Fermi surface $p_F(x)$ multivalued at large enough times ($t > t_c$) and leads to the appearance of infinite spatial gradients of fermionic density (Fig. 2, top and middle panels). This suggests that the simple semiclassical descriptions (6) and (5) may become insufficient beyond the time t_c when the shock occurs, raising the question of what happens with the density profile at $t > t_c$.

We have performed direct quantum simulations of this problem by using a tight-binding free-fermion model. The top panel of Fig. 3 demonstrates the density evolution from initial state with a density hump at $t = 0$ (top left panel) to state at certain time after the shock (approximately five times larger than t_c). At $t > 0$, only the right-moving part of the density pulse is shown. A full movie of density evolution is available in the Supplemental Material.[14] The initial density perturbation was approximately Gaussian:[15]

$$\rho_0(x) = \rho_\infty + \frac{N}{\sqrt{2\pi\sigma^2}} e^{-x^2/2\sigma^2} \quad (7)$$

with dispersion σ of about 100 lattice sites and contained $N \approx 12.8$ electrons. The density of the underlying Fermi sea is 0.2 fermions per site, so that the cosine-shaped dispersion relation of the tight-binding model can be well approximated by a parabola. The bottom panel of Fig. 3 shows the evolution of a Gaussian density dip with approximately the same parameters $\sigma \approx 95$ and $N \approx -14.7$.

For convenience of the reader, the snapshot of the density at $t \approx 5t_c$ (for initial density hump) is also shown in the bottom panel of Fig. 2. By comparing the exact quantum result (Fig. 2, bottom) to the naive semiclassical result dictated by the Euler equation (Fig. 2, middle), we see that the shock gets regularized via the onset of pronounced density oscillations at the front edge of the pulse. It is important to emphasize that the period of those oscillations is controlled by the amplitude $\Delta\rho$ of the density perturbation and is thus much larger than

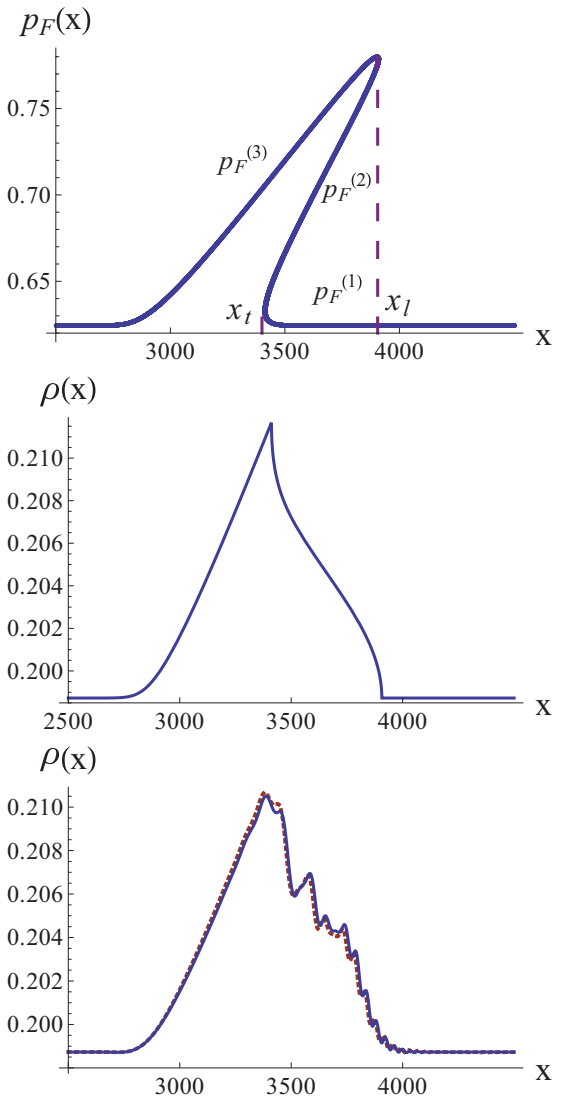

FIG. 2. (Color online) Top: Quasiclassical phase-space distribution as obtained from the Euler equation at $t \approx 5t_c$. In-between trailing and leading edges x_t and x_l, the Fermi surface is multivalued with branches $p_F^{(i)}$, $i = 1,2,3$. Middle: Naive quasiclassical approximation to the density profile as obtained by momentum integration of the phase-space distribution shown in the top panel. Bottom: Snapshot of fermionic density $t \approx 5t_c$ as obtained from direct numerical simulations of free fermions on a lattice. The initial density pulse was Gaussian (see main text and Fig. 3). The dots show the semiclassical result derived in Sec. II B.

λ_F. (We will perform a detailed quantitative analysis of the oscillation period in Sec. II B.) From this point of view, the developing oscillations may be considered as quasiclassical: their characteristic scale is much larger than λ_F. Thus, a smooth initial density stays smooth at scale λ_F also at times after the "shock."

The evolution of the density dip shown in the bottom panel of Fig. 3 is very similar to the one of the density hump. The only difference is that the shock and the oscillations develop now at the rear side of the pulse. For definiteness, we focus on the case of density hump in the subsequent discussion.

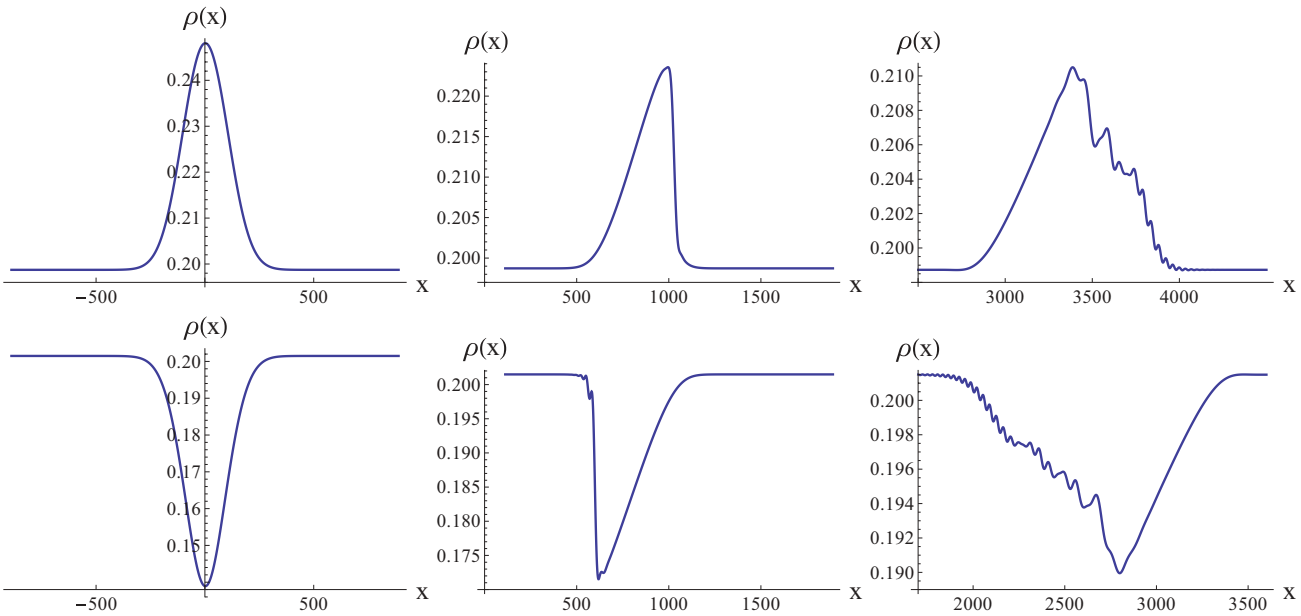

FIG. 3. (Color online) Evolution of the fermionic density (measured in fermions per site) as obtained from direct numerical simulations of free fermions on a lattice. The unit of length is set by the lattice constant. Top left: The initial density pulse has Gaussian shape with the amplitude $\Delta\rho \approx 0.05$ and the dispersion $\Delta x \approx 102.6$, comprising 12.8 electrons. Top middle: Density profile at t slightly smaller than the "shock" time t_c. Only right-moving part is shown. The front edge of the pulse has become steep, but the overturn has not yet occurred. Top right: Fermionic density after the "shock" $t \approx 5t_c$. Density ripples develop at front edge. Bottom: Evolution of fermionic density for density dip in the initial state. The parameters of the initial perturbation are close to that of the top panel. The pulse comprises 14.9 holes and has width of $\Delta x \approx 95.7$. The subsequent density evolution is very similar to the case of the density hump. The "shock" and the density ripples develop at the back edge of the pulse.

We thus face an apparent contradiction: the density profile remains "quasiclassical" (smooth on the scale of λ_F) after the shock but develops strong oscillations that are not caught by the quasiclassical approximation based on Eqs. (5) and (6). The resolution of this "paradox" is related to the fact that Eq. (5) is not the fully correct semiclassical (in the above sense) approximation for the Wigner function of fermions in a smooth potential well. As was pointed out in Ref. 16, instead of having an abrupt drop from 1 to 0 at Fermi momentum, $f_0(X,p)$ as a function of p develops oscillations near $p_F(X)$. Those oscillations can be considered as a semiclassical effect in the sense that their form knows nothing about λ_F and is controlled solely by the derivatives of $p_F(X)$. In Sec. II B, we give a detailed account of the oscillations in the Wigner function and of their implications for the density evolution.

B. Wigner function of fermions in a potential well and density oscillations

The Wigner function $f_0(p,X)$ of the initial state satisfies the equation

$$\partial_X \partial_y f_0(X,y) - [U(X_+) - U(X_-)]\, f_0(X,y) = 0\,, \qquad (8)$$

where the coordinate y is conjugate (in the sense of Fourier transformation) to the momentum p [cf. Eq. (2)]. As we are interested in the behavior of $f_0(p,X)$ close to one of the Fermi edges $p = \pm p_\infty$ we can replace ∂_y by ip_∞ (we concentrate here on the right Fermi edge). This corresponds to taking the limit $p_\infty \to \infty$ while keeping the profile $p_F(x) - p_\infty$ fixed. Solving the resulting equation

$$\partial_X f_0(X,y) - i\,[p_F(X_+) - p_F(X_-)]\, f_0(X,y) = 0\,, \qquad (9)$$

with the condition at infinity

$$f_0(X = -\infty, y) = \int \frac{dp}{2\pi} e^{ipy} \Theta\,(p_\infty - p) \qquad (10)$$

and transforming the result to momentum space, we find in agreement with Ref. 16

$$f_0(X,p) = \int \frac{dy}{2\pi i (y - i0)} e^{-iS[y;X,p]}, \qquad (11)$$

$$S[y;X,p] = py - \int_{X-\frac{y}{2}}^{X+\frac{y}{2}} dX' p_F(X'). \qquad (12)$$

Note that our approach is slightly different from that of Ref. 16: we consider an equilibrium state in a potential $U(x)$, while the authors of Ref. 16 construct a coherent state by acting on the homogeneous Fermi vacuum with an exponential of a bilinear in fermionic operators.

The general structure of the Wigner function can be inferred from Eqs. (11) and (12) by performing the integration with making use of the saddle-point method. The saddle-point equation for the action (12)

$$p = \frac{p_F(X + y/2) + p_F(X - y/2)}{2} \qquad (13)$$

has no real-valued solutions for $p < p_\infty$ or

$$p > p_{\max}(x) \equiv \max_y \frac{p_F(X + y/2) + p_F(X - y/2)}{2}. \qquad (14)$$

In these parts of the phase space, the integral (11) is controlled by the singularity at $y = 0$, and $f_0(X,p)$ can be well approximated by the Heaviside Θ function.

On the contrary, for $p_\infty < p < p_{\max}(X)$ there exist (at least) two solutions $y = \pm y^*(X,p)$ to the saddle-point equation providing an oscillatory contribution to the Wigner function

$$\delta f_0(X,p) \propto \mathrm{Re}[Ae^{-iS[X,p]}]. \tag{15}$$

Here, A is the coefficient controlled by the fluctuations around the saddle points. The phase of oscillations is given by $S[X,p] = S[y^*(X,p);X,p]$. It defines the period of oscillations with the momentum via $S[X,p+\Delta p] - S[X,p] = 2\pi$. Counting the powers of imaginary unit in the saddle-point integration, one easily finds that the maxima of the Wigner function appear at $S[X,p] = -3\pi/4 \ \mathrm{mod} 2\pi$.

In a sufficiently close vicinity of the local Fermi surface $|p - p_F(x)| \ll p_F(0) - p_\infty$, one can locally approximate $p_F(x)$ by a parabola and express the Wigner function $f_0(x,p)$ in terms of the Airy function.[16] This approximation is, however, insufficient for our purposes, as the density oscillations will originate from Wigner function oscillations at all scales $|p - p_F(x)| \sim p_F(0) - p_\infty$.

The oscillatory behavior of $f_0(X,p)$ is illustrated in Fig. 4 where we plot $f(X=0,p)$ [calculated via numerical integration of Eq. (11)] as a function of momentum. To generate the plot, we have assumed the Gaussian density used in the quantum simulations presented in Sec. II A and in Fig. 3. A straightforward analysis of the saddle-point equation shows that, upon variation of momentum from $p = p_{\max}(0) = p_F(0)$ to p_∞, $S[X=0,p]$ varies monotonically from 0 to $-2\pi N$, where

$$N = \frac{1}{2\pi}\int dx[p_F(x) - p_\infty] \tag{16}$$

is (generally noninteger) the number of particles in the pulse. Accordingly, the Wigner function of Fig. 4 shows six oscillations corresponding to approximately six right-moving particles. Vertical lines in Fig. 4 mark the momenta satisfying the condition $S[X,p] = -3\pi/4 \ \mathrm{mod} 2\pi$.

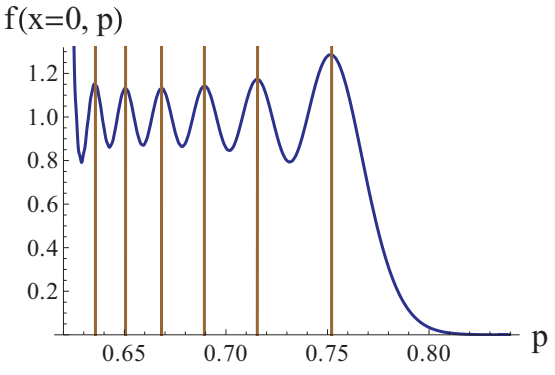

FIG. 4. (Color online) Initial-state Wigner function $f_0(X=0,p)$ as obtained via numerical integration of Eq. (11). The same Gaussian density profile as used in the quantum simulations presented in Sec. II A and in Fig. 3 was assumed. The observed six oscillations correspond to 6.4 right-moving particles in the pulse. Vertical lines mark the momenta satisfying the condition for oscillation maxima $S[X,p] = -3\pi/4 \ \mathrm{mod} 2\pi$.

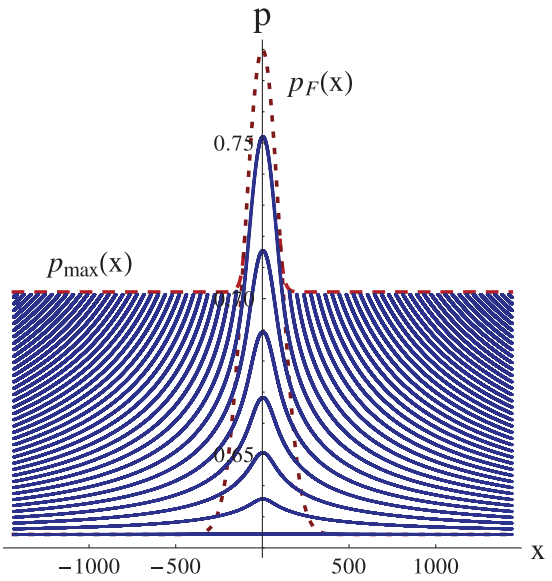

FIG. 5. (Color online) Phase-space oscillations of the Wigner function $f_0(x,p)$ for the initial state [the same Gaussian density hump as in the previous figures; the corresponding $p_F(x)$ is shown by dotted line]. Blue solid lines are contours of constant action (which determines the phase of the Wigner function) $S[X,p] = -3\pi/4 \ \mathrm{mod} 2\pi$. Dashed line represents the border $p_{\max}(x)$ of the region of developed oscillations.

The overall behavior of $f_0(X,p)$ in the phase space can be conveniently represented by lines of constant action $S[X,p]$. For the case of Gaussian density, the corresponding pictures are shown on Fig. 5. The green dashed line here represents the border $p_{\max}(x)$ of the region of developed oscillations. The solid blue lines are the lines of constant action $S[X,p] = -3\pi/4 \ \mathrm{mod} 2\pi$. Finally, the dotted line shows the x-dependent Fermi level. The "topology" of the plot can be understood on general grounds and does not depend on the specific density $\rho_0(x)$. At large X, the action is a steep function of momentum p and, when taken modulo 2π, acquires any given value many times. Among the lines of constant action coming from $X = +\infty$, exactly $[N]$ (this denotes the integer part of N) lines cross the p axes and flow to $X = -\infty$, while other lines end up on the border $p = p_{\max}(x)$ where the solution $y^*(X,p)$ to the saddle-point equation becomes complex.

Let us now discuss the implications of the above results for the fermionic density which is equal to the integral over momentum of the Wigner function. In the initial state, the density is insensitive to the oscillations of the Wigner function. Indeed, one can observe that the contour of momentum integration (vertical line on Fig. 5) crosses many contours of constant $S[X,p]$ but does not touch any of them, so that there is no stationary-point contribution to the integral. In fact, evaluating the p integral of Eq. (11), we find that in the considered (large-p_F) approximation, the equality $\rho_0(x) = p_F(x)/\pi$ is exact.

The evolution of each contour line of the action is governed by the Euler equation (6). The behavior of the Wigner function after the shock, $t > t_c$, is illustrated by Fig. 6. Now the vertical

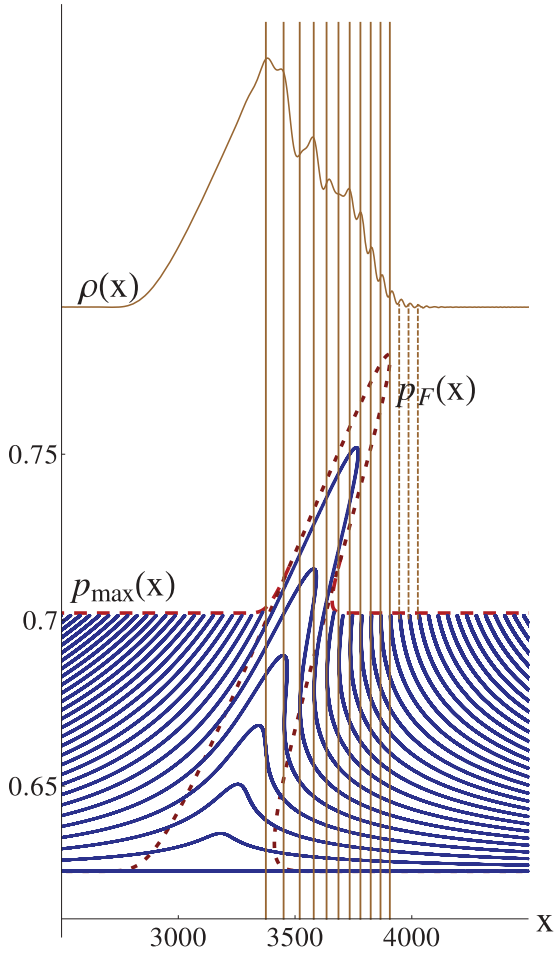

FIG. 6. (Color online) Top: Density profile after the shock as obtained by numerical numerical integration of the Wigner function (11). The result is almost indistinguishable from that of first-principles quantum simulations shown in Fig. 2. Bottom: The same as in Fig. 5 but after evolution beyond the shock. All parameters, including the evolution time, are the same as in the upper plot and in Fig. 2. The vertical lines touching the constant-action contours mark stationary-point contributions to the momentum integral of the Wigner function and thus determine maxima of the density oscillations in the upper plot.

lines do touch the contours of constant action. A touching point becomes the saddle point for the integration over momentum and the oscillations in $f_0(X,p)$ start to contribute to the density. This implies a maximum in the density each time the integration line touches the contour line corresponding to $S[X,p] = -3\pi/4 \bmod 2\pi$.

The curve in the upper part of Fig. 6 shows the density obtained via numerical integration of the Wigner function (11). This is almost indistinguishable from the result of first-principles quantum simulations (bottom panel of Fig. 2). We observe that the positions of the maxima of the density are in accord with the above argument based on the saddle-point approximation.

One can now determine the period of the density modulations. Let us focus on the region closer to the front edge of the pulse where the oscillations are clearly governed by a single harmonics (see Fig. 2), and are perfectly described by the saddle-point argument as shown in Fig. 6. As this figure further illustrates, the integration contour touches the contour lines near $p = p_{\max}(X)$ and the period of the density oscillations is set by $S[X, p = p_{\max}(X)]$. In this regime, we have

$$y^*[X, p_{\max}(X)] \simeq 2X, \quad p_{\max}(X) \simeq \frac{p_F(0) + p_\infty}{2}. \tag{17}$$

Thus, $S[X, p_{\max}(X)] \simeq [p_F(0) - p_\infty]X$ and we immediately infer the period

$$\delta X \simeq \frac{2\pi}{p_F(0) - p_\infty}. \tag{18}$$

It is not difficult to generalize this argument to the region closer to the top of the pulse. Assuming for simplicity that the time that has passed after shock is of the order of the shock time $t_c \sim m\Delta x/\Delta\rho$, we find that the characteristic spatial scale for the first few oscillations (just to the right of the maximum of the pulse) is larger than (18) by a factor $\sim N^{1/3}$ (for the parameters used in our plots, this is approximately 2). Some complication comes from the fact that in this region a superposition of oscillations originating from different regions in phase space takes place. Indeed, as is clearly seen in the lower panel of Fig. 6, constant-action contours that do not terminate at $p_{\max}(x)$ may have two points with infinite slope, and each of them will give a stationary-phase contribution when the momentum integration is performed. This superposition explains a somewhat irregular oscillation pattern in the corresponding spatial region.

The obtained oscillations can be interpreted as Friedel-type oscillations between different branches of the Fermi momentum (that becomes multivalued after the "shock"). In particular, in the front region, the upper two branches are close to the maximum value $p_0(0)$, while the lower branch is essentially equal to p_∞, which yields exactly Eq. (18).

Quasiclassical analysis of Sec. II B can be straightforwardly modified to the case of density dip. The results are in full agreement to quantum simulations (see lower panel of Fig. 3).

III. HYDRODYNAMICS OF FREE FERMIONS

The analysis of the previous section provides a detailed description of the evolution of coherent perturbation in the density of free fermions. The analysis is complete and, as was also confirmed by numerical simulations, essentially exact under our basic assumptions. It is appealing, however, to try to formulate a hydrodynamic description of the problem which, in contrast to the fermionic approach utilizing the notion of Wigner function, would involve as fundamental objects only the density and the velocity of the electronic fluid. Indeed, the hydrodynamics (bosonization) constitutes a convenient and powerful framework for the discussion of interaction effects (to be considered in Sec. IV), which are otherwise hard to access.

Usually, hydrodynamics rests on the assumption of local equilibrium forced by the particle collisions which wash out any features in the particle distribution function. In the present problem, no such equilibrium exists. Moreover, we saw above that the oscillating behavior of $f(p)$ is crucial for the density

ripples observed in the shock region. Hence, one can expect that the evolution of the quantum-coherent many-particle state can not be controllably described by classical equations of hydrodynamic type. Despite this fact, one can ask if it is possible to design phenomenological hydrodynamic equations which would capture qualitative features of the true density evolution. In this section, we show that this is indeed possible and such phenomenological equations provide important insight into the physics of nonequilibrium many-particle systems.

In our search for hydrodynamics, it is convenient to start from the Euler equation (6) corresponding to the neglect of all oscillatory features in the Wigner function $f_0(X,p)$. Combined with analogous equation for the Fermi surface of left electrons at $t < t_c$, it can be rephrased in terms of the mean density and velocity of the fluid as

$$\partial_t \rho + \partial_x(\rho v) = 0\,, \quad \partial_t v + \partial_x\left(\frac{v^2}{2} + \frac{\pi^2\rho^2}{2}\right) = 0, \tag{19}$$

$$\rho(x) = \int \frac{dp}{2\pi} f(x,p)\,, \quad v(x) = \frac{1}{\rho(x)}\int \frac{dp}{2\pi} p f(x,p). \tag{20}$$

Of course, Eqs. (19) suffer from the same shock phenomenon as the original equation (6). Phenomenologically, we would like to add some terms to Eq. (19) regularizing the shock instability. We know that regularization goes through the onset of density ripples in the shock region. This phenomenon is well known in hydrodynamics and is usually referred to as "dispersive regularization."[17] It takes place when the shock caused by nonlinearity gets regularized by higher-order derivatives consistent with the time-reversal invariance of the equations. The classical examples are the Korteweg–de Vries (KdV) and Gross-Pitaevskii equations. It is the requirement of time reversal that makes the "dispersive regularization" very different from "dissipative regularization" achieved by the introduction into the system of some type of viscosity. Examples of the latter type are Navier-Stokes and Burgers equations.

Let us now point out that Eqs. (19) appear in the theory of Fermi gas in yet another context and with slightly different meaning. Specifically, the standard bosonization procedure applied to the fermions with quadratic spectrum leads to Hamiltonian[18–22]

$$\hat{H} = \int dx \left(\frac{\widehat{v\rho v}}{2} + \frac{\pi^2\widehat{\rho}^3}{6}\right). \tag{21}$$

Here, $\widehat{\rho}$ and $\widehat{v}$ are *operators* with the commutation relations

$$[\widehat{\rho}(x),\widehat{v}(y)] = -i\delta'(x-y). \tag{22}$$

The Hamiltonian and the commutation relations imply the operator equations of motion usually referred to as "quantum Euler equations"

$$\partial_t\widehat{\rho} + \partial_x(\widehat{\rho v}) = 0\,, \quad \partial_t\widehat{v} + \partial_x\left(\frac{\widehat{v}^2}{2} + \frac{\pi^2\widehat{\rho}^2}{2}\right) = 0. \tag{23}$$

One can now see that there exist two sources of corrections to hydrodynamic equations (19). First, there can be corrections to the quantum Hamiltonian (21) missed by the bosonization in its simplified form. If present, they would yield a direct contribution to the quantum Euler equations (23). Second, passing from quantum equations (23) to identically looking classical equations (19) implies averaging of the former over the quantum state. In the functional integral formulation of the problem, classical equations (19) correspond to the saddle-point treatment of the functional integration. However, loop corrections can also contribute to the average density and current and generate new terms in Eq. (19). In the following, we discuss both aforementioned effects.

A. Correction to Hamiltonian

Let us first explore corrections to the Hamiltonian (21). For a while, we put the loop corrections aside (we will return to them in Sec. III B) and thus make no distinction between classical and quantum equations of motion.

We start with Haldane's theory[23] that accounts for a discrete nature of particles as well as for their spectrum.[24] Within this model, the fermionic operator is represented by an infinite sum

$$\hat{\Psi}(x) = \sqrt{\hat{\rho}}e^{i\hat{\theta}(x)}\left(\sum_{l\ \mathrm{odd}} e^{-il\pi\hat{\phi}(x)}\right), \tag{24}$$

where the bosonic fields have the standard commutation relations

$$[\hat{\theta}(x),\hat{\phi}(x')] = -\frac{i}{2}\mathrm{sgn}(\mathrm{x}-\mathrm{x}'), \tag{25}$$

and are related to the velocity and density fields as

$$\hat{v}(x) = \partial_x\hat{\theta}(x)\,, \quad \hat{\rho}(x) = \partial_x\hat{\phi}(x). \tag{26}$$

After substituting Eq. (24) into the free Hamiltonian

$$\hat{H} = -\frac{1}{2}\int dx\ \hat{\Psi}^+(x)\nabla^2\hat{\Psi}(x), \tag{27}$$

one obtains

$$\hat{H} = \frac{1}{2}\int dx \sum_{l\ \mathrm{odd}}\left(\hat{\theta}_x\hat{\rho}\hat{\theta}_x + \pi^2 l^2\hat{\rho}^3 + \frac{1}{4}\frac{\hat{\rho}_x^2}{\hat{\rho}}\right). \tag{28}$$

This result contains an infinite summation over odd integers l, and formally diverges. To properly define this series, one needs to regularize the divergent sums. This can be achieved by describing the series as an expansion of an analytic function of some argument [$y(z) = \sum_l y_l z^l$]. A series of this type has to be summed within the range of its convergence and then analytically continued to $z = 1$. Bearing such a procedure in mind and comparing Eq. (28) with Eq. (21), we establish that such regularization implies

$$\sum_{l\ \mathrm{odd}} 1 = 1 \quad \text{and} \quad \sum_{l\ \mathrm{odd}} l^2 = \frac{1}{3}\,. \tag{29}$$

Thus, one obtains

$$\hat{H} = \int dx \left(\frac{1}{2}\hat{v}\hat{\rho}\hat{v} + \frac{\pi^2\hat{\rho}^3}{6} + \frac{1}{8}\frac{\hat{\rho}_x^2}{\hat{\rho}}\right). \tag{30}$$

The first two terms in Eq. (30) are contained in the Hamiltonian (28). However, the last term in Eq. (30) represents the gradient corrections that are beyond the Hamiltonian (28). Note that although the derivation outlined above may not appear rigorous, there is no ambiguity in determining the

last term in Eq. (30). Indeed, the regularization procedure we use is fully determined by the first two terms in the Hamiltonian. Therefore, the coefficient in front of the third term is unambiguously determined. The Hamiltonian (30) leads to the following equations of motion:

$$\partial_t \hat{\rho} + \partial_x(\hat{\rho}\hat{v}) = 0\,, \quad \partial_t \hat{v} + \hat{v}\partial_x \hat{v} + \partial_x \hat{w} = 0\,. \tag{31}$$

Here,

$$\hat{w} = \frac{\pi^2\hat{\rho}^2}{2} - \frac{1}{4}\partial_x^2 \ln\hat{\rho} - \frac{1}{8}(\partial_x \ln\hat{\rho})^2 \tag{32}$$

is the enthalpy of the Fermi gas. The first term in Eq. (32) is the pressure of a homogeneous Fermi gas, while the last two terms describe the cyclotronic pressure that accounts for the finite density gradient. Interestingly enough, this latter contribution is quite universal and appears also in the Madelung fluid[1] as well as in the hydrodynamic form of the Gross-Pitaevskii equation.[17] The presence of the finite gradient terms stabilizes the classical equation of motions. Thus, it is natural to ask a question whether Eqs. (31) and (32) are sufficient to describe the evolution of the density pulse discussed in Sec. II A.

To answer this question, we simulate the evolution of the density pulse (7) in accordance with Eq. (32). The results of this analysis shown in Fig. 7 clearly indicate the formation of a region of oscillations in the density profile. However, the period of the oscillations is parametrically different from that obtained from the direct quantum-mechanical solution of the free-fermion problem of Sec. II (see Appendix A for details). Indeed, the spatial scale of the oscillations is determined by the competition between the nonlinearity and the dispersion. In the present case, a simple estimate gives

$$\delta x \sim \frac{1}{\sqrt{\rho_\infty \Delta\rho}} \sim \sqrt{\frac{\lambda_F}{\Delta\rho}}. \tag{33}$$

This is smaller by a factor $(\lambda_F \Delta\rho)^{1/2} \ll 1$ than the result (18) of the direct solution of the free-fermion problem. We thus conclude that Eqs. (31) and (32) yield a *parametrically wrong* scale for the density ripples: the dispersive term in Eqs. (30)

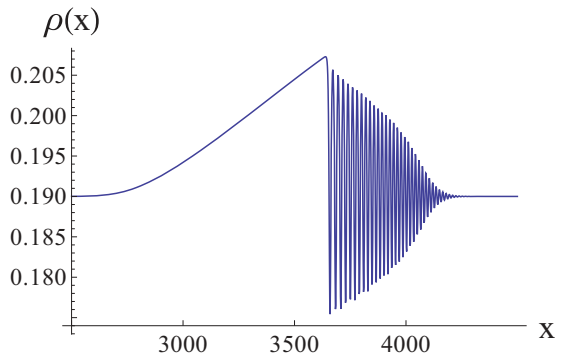

FIG. 7. (Color online) Results of numerical solution of hydrodynamic equations (31) and (32). The initial density pulse was Gaussian with the parameters used previously in Sec. II. The period of oscillations induced by the shock is determined by the competition between dispersion and nonlinearity, $\delta x \sim \sqrt{\lambda_F/\Delta\rho}$. It is parametrically smaller than the one found in Sec. II within a direct analysis of the free-fermion problem.

and (32) is too weak. Thus, in our search for hydrodynamics, we must resort to loop corrections to the equations of motion.

Before passing to the analysis of loop corrections, let us make the following comment. While the dispersive term in Eq. (30) turns out to be parametrically small in comparison to quantum effects for free fermions, such a term (with a parametrically enhanced prefactor) will become a dominant dispersive term for the case of electrons with finite-range interaction with a sufficiently large interaction radius (see Sec. IV A). Consequently, the semiclassical analysis of Eq. (30) (with an appropriately modified coefficient of the last term) performed above and in Appendix A will become a controllable description in that case, as discussed in Sec. IV A.

B. Loop corrections

Let us follow our phenomenological approach and try to guess the form of the loop corrections to the enthalpy (32) on the basis of our knowledge of the characteristic scale of the ripples. It is easy to see that to produce the correct period of the density oscillations, the correction should scale as first power of momentum. A simple term of the form $\partial_x\rho$ is not acceptable as it would break the symmetry with respect to the spatial inversion. This symmetry can be saved, however, by inclusion of the Hilbert transform $\widehat{\mathcal{H}}$,

$$\delta w \sim \widehat{\mathcal{H}}\partial_x \rho. \tag{34}$$

By definition, in the momentum domain, the Hilbert transform acts according to $\widehat{\mathcal{H}}\rho_k = -i\pi\,\mathrm{sign}(k)\rho_k$. From now on, we denote by symbols with hats the operators acting on functions of x (like Hilbert transform above) and omit the hats over operators acting in Hilbert space. We reserve a special notation $\widehat{A}_2$ for the operator $\widehat{\mathcal{H}}\partial_x$. The reason for such a notation will become clear in Sec. IV. In momentum space,

$$\widehat{A}_2\rho_k = \pi|k|\rho_k. \tag{35}$$

The enthalpy corrections of the form (34) were first suggested by Jevicki[25] in his study of the ρ^3 theory defined by the the Hamiltonian (21). He pointed out that such a theory contains two single-particle branches. In fermionic language, these correspond to the electron and hole parts of the spectrum,

$$\epsilon_{p(h)} = k_F|k| \pm \frac{k^2}{2}, \tag{36}$$

with subscripts p and h referring to particles and holes, respectively. Further, it was observed in Ref. 25 that each of the Lagrangians

$$L_{p(h)} = \int dx \left(\frac{1}{2}\frac{\phi_t^2}{\phi_x} - \frac{1}{8}\frac{\phi_{xx}^2}{\phi_x} - \frac{\pi^2}{6}\phi_x^3 \mp \frac{1}{2}\phi_x \widehat{A}_2 \phi_x\right), \tag{37}$$

$$\phi = \partial_x^{-1}\rho \tag{38}$$

when treated semiclassically (i.e., on the saddle-point level), reproduces correctly the dispersion relation for the corresponding branch of excitations (36). In other words, Eq. (37) is an effective semiclassical theory that takes into account explicitly quantum corrections of the original cubic theory (21).

The term with the Hilbert transform in Eq. (37) gives rise to k^2 correction to the linear spectrum of the conventional bosonization [see Eq. (36)]. It is known that loops in the perturbative diagrammatic treatment (in the context of

equilibrium problems) of the Hamiltonian (21) lead indeed to such an effect.[26,27] Specifically, with loops taken into account, the support of the bosonic spectral weight in the (ω,k) plane, which is just a line $\omega = k_F k$ for the linear electronic spectrum, starts to receive a finite width[28] of order k^2. We thus see that the inclusion of the term (34) into the enthalpy is a natural way to simulate the effect of loop corrections.

Motivated by these findings, we try to apply the effective semiclassical Lagrangians (37) to our problem. At this point, a question naturally arises: which of the two Lagrangians L_p, L_h should we choose [i.e., which sign should we choose in Eq. (37)]? We argue here in the following way. Let us assume that the original density perturbation is positive, i.e, has a form of a hump as shown in Fig. 1. Such a perturbation can be obtained by generating particle excitations on top of a homogeneous vacuum state. Therefore, we choose the Lagrangian L_p as appropriate in this situation. Similarly, in the case of a diplike (i.e, negative) density perturbation, the Lagrangian L_h should be taken. This choice is by no means innocent, as will be discussed in more detail in the following.

For definiteness, we consider a humplike excitation (as was also done in Sec. II) and thus the Lagrangian L_p. Corresponding hydrodynamic equations (31) with the enthalpy

$$w = \frac{\pi^2\rho^2}{2} - \frac{1}{4}\partial_x^2 \ln\rho - \frac{1}{8}(\partial_x \ln\rho)^2 + \widehat{A}\rho \qquad (39)$$

are of the Benjamin-Ono type. They were studied previously in the literature in the context of the Calogero model (see Sec. IV B). In Sec. III C, we analyze these equations and compare the outcome to the result of the fermionic solution presented in Sec. II B.

C. Nonlocal hydrodynamics of free fermions

As a first step of our analysis of the classical hydrodynamics defined by Eqs. (31) and (39), we have performed their numerical simulations for the initial density used previously in our quantum computations. The result is shown in Fig. 8. The dashed vertical lines mark the positions of the maxima in the exact fermionic density analyzed in Sec. II (the same lines as in Fig. 6). We observe a very good agreement between the free-fermion problem and the classical hydrodynamics (31) and (39) in the period of the oscillations induced by the shock. The agreement becomes perfect closer to the front edge of the impulse.

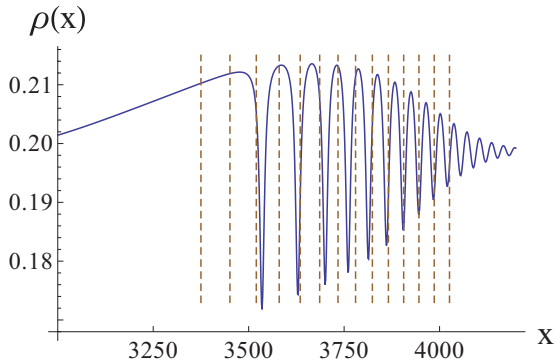

FIG. 8. (Color online) Results of numerical solution of the semiclassical hydrodynamic equations (31) and (39). Vertical lines mark the positions of density maxima in the exact quantum-mechanical result for free fermions (see Sec. II). The oscillation periods perfectly agree in the front part of the pulse [see Eqs. (18) and (56)]. Near the top of the pulse, the periods experience parametrically the same ($\sim N^{1/3}$) enhancement in both cases but somewhat differ numerically.

To explore analytically the oscillations emerging in the hydrodynamics (31) and (39) at times exceeding the shock time t_c, we employ the Whitham modulation theory.[13] Within this approach, one considers the solution to hydrodynamic equations in the shock region (the interval between the points x_l and x_t of Fig. 2 as a periodic single-phase wave with slowly modulated parameters (wave vector, frequency amplitude, etc.). The modulation equations for those parameters are obtained from the Lagrangian averaged over a period of oscillations. For the Lagrangian L_p, the single-phase periodic wave was found in Ref. 39:

$$\phi(x,t) = \rho_0 x - \gamma t + \Phi(\theta), \quad \theta = kx - \omega t. \qquad (40)$$

Here, ρ_0 and γ represent mean density and the current in the wave; k and ω are the wave vector and frequency, and 2π-periodic function $\Phi(\theta)$ is defined by its derivative

$$\dot{\Phi} = \frac{1}{2\pi}\left(1 - \frac{\sinh a}{\cosh a - \cos\theta}\right), \qquad (41)$$

$$\tanh a = \frac{4\pi k^3\rho_1^3}{k^4\rho_1^2 + 4\pi^2 k^2\rho_1^4 - 4(k\gamma - \omega\rho_0)^2}, \qquad (42)$$

$$\rho_1 = \rho_0 + \frac{k}{2\pi}. \qquad (43)$$

The density in the wave $\rho = \partial_x\phi$ reads as

$$\rho = \rho_1 - \frac{k}{2\pi}\frac{\sinh a}{\cosh a - \cos\theta}. \qquad (44)$$

The parameter a controls the amplitude of the periodic wave

$$A = \frac{\rho_{\max} - \rho_{\min}}{2} = \frac{k}{2\pi\sinh a}, \qquad (45)$$

as well as its shape. In the limit $a \gg 1$, Eq. (44) reduces to weak harmonic oscillations, while in the opposite limit $a \ll 1$, one gets a train of well-separated solitons, each of them carrying exactly one electron.

The modulation equations for parameters γ, ρ_0, k, and ω were derived in Ref. 29 where a specific (Lorentzian) form of the original pulse was used (see also Refs. 30 and 31 for the discussion of modulation equations for a closely related Benjamin-Ono equation). In Appendix B, we present a general derivation of modulation equations. The result is conveniently presented in terms of four Riemann invariants u_i satisfying

$$\partial_t u_i + u_i\partial_x u_i = 0, \quad i = 0,\ldots,4. \qquad (46)$$

The parameters of the wave are given by

$$k = u_2 - u_1, \qquad (47)$$

$$\omega = \frac{1}{2}(u_2^2 - u_1^2), \qquad (48)$$

$$\rho_0 = \frac{u_3 - u_2 + u_1 - u_0}{2\pi}, \qquad (49)$$

$$\gamma = \frac{-u_0^2 + u_1^2 - u_2^2 + u_3^2}{4\pi}. \qquad (50)$$

The modulation equations should be supplemented by the boundary conditions at the ends of the shock region x_t and x_l. These conditions consist of the requirement that the average density and current ρ_0 and γ match those dictated by the Euler equation (6) in the regions without population inversion ($x < x_l$ and $x > x_t$). We thus have

$$\rho_0 = \frac{p_F^{(3)} + p_\infty}{2\pi}, \quad \gamma = \frac{\left(p_F^{(3)}\right)^2 - p_\infty^2}{4\pi}, \quad x = x_t \tag{51}$$

$$\rho_0 = \frac{p_F^{(1)} + p_\infty}{2\pi}, \quad \gamma = \frac{\left(p_F^{(1)}\right)^2 - p_\infty^2}{4\pi}, \quad x = x_l \tag{52}$$

where we used the notation $p_F^{(i)}$ introduced for three branches of the Fermi momentum in Sec. II (see Fig. 2). The solution of the equations for Riemann invariants with these boundary conditions is given by

$$u_i = p_F^{(i)}, \quad i = 1,2,3 \tag{53}$$

$$u_0 = -p_\infty. \tag{54}$$

The modulation theory described above reveals a deep connection between the hydrodynamic system [Eqs. (31) and (39)] and the free fermions. Indeed, according to Eq. (53), the Riemann invariants u_i, $i = 1,2,3$, characterizing hydrodynamic density oscillations in the shock region are exactly equal to three branches $p_F^{(i)}$ of the Fermi surface of free fermions in the population-inversion regime. Furthermore, the equipotential lines of the action $S[X,p]$ that played a central role in our "fermionic analysis" of the density ripples evolve according to exactly the same Euler equation (6) as that for Riemann invariants [Eq. (46)].

Equations (47) and (53) allow us to make a precise statement on the period of oscillations:

$$\delta x = \frac{2\pi}{p_F^{(2)} - p_F^{(1)}}. \tag{55}$$

Thus, we see that close to the front end of the pulse the period is

$$\delta x = \frac{2}{\Delta\rho} \tag{56}$$

and coincides exactly with that of the density oscillations for the exact quantum-mechanical solution of the free-fermion problem [see Eq. (18)]. It is easy to see that near the top of the pulse the period is larger by a factor $\sim N^{1/3}$ (assuming for simplicity that the time $t - t_c$ that has passed after the shock is of order t_c), again in agreement with the analysis of Sec. II B. Equation (55) is fully consistent with the interpretation of the oscillatory structure as Friedel oscillations between different Fermi-momentum branches.

The following comment is in order here. As has been explained above, when the hydrodynamic theory [Eqs. (31) and (39)] is used to describe the behavior of free fermions, the choice of the particle branch L_p in Eq. (37) captures essential features of the evolution of a density *hump*, while the hole-branch Lagrangian L_h is appropriate for a density *dip*. On the other hand, if we would try to apply, e.g., L_h for a density hump, it would fail completely. Specifically, it would predict the formation of the solitonic train in front of the running pulse, i.e., a decomposition of the initial density perturbation into well-separated solitons (cf. Sec. IV B), which never happens for free fermions. It remains an open question as to whether there exists an improved hydrodynamic theory that describes evolution of the free-fermion density perturbation consisting of a combination of humps and dips. In this context, it is also worth reminding the reader about the following. While the classical hydrodynamics analyzed in this section perfectly reproduces the period of free-fermion oscillations induced by a shock, it considerably overestimates their amplitude. If there exists a better hydrodynamic description of this problem, one might hope that it would be free also of this drawback.

IV. INTERACTION EFFECTS

In the previous sections, we discussed the evolution of the density perturbation in the free-electron gas within (i) the exact "fermionic" approach and (ii) the phenomenological hydrodynamics. We concluded that, in the latter formalism, quantum loop corrections are crucial in determining the character of the dispersive regularization of the shock. They can be modeled qualitatively by the nonlocal term (34) in the enthalpy of free fermions. At this level, the bosonized Hamiltonian for free fermions [that corresponds to the effective Lagrangian (37)] takes the form (different for particlelike and holelike perturbations)

$$H_{p(h)} = \int dx \left[\frac{1}{2}\rho v^2 + \frac{\pi^2\rho^3}{6} + \frac{1}{8}\frac{\rho_x^2}{\rho} \pm \frac{1}{2}\rho\widehat{A}_2\rho\right]. \tag{57}$$

The term with ρ_x^2 coming from Haldane bosonization prescription is not important in the low-gradient limit.

In this section, we discuss modifications of the picture drawn above that arise due to the electron-electron interaction. From the perspective of the "fermionic" solution of Sec. II B, one obvious consequence of the interaction is the appearance of energy relaxation leading to local thermalization of the distribution function. This thermalization will eventually wash out all the oscillating features of the density. However, the corresponding time will be very large since the lifetime of electronic excitations in an interacting 1D system scales as a high power of the mass m (inverse curvature of the spectrum near the Fermi points) or, equivalently, of the Fermi momentum $p_F = mv_F$ (see Ref. 8 for a review). Specifically, at zero temperature the lifetime of a quasiparticle with momentum k due to a long-range (smooth on the scale λ_F) electron-electron interaction $V(r)$ is given by[8,9]

$$\frac{1}{\tau_p} \sim \left[V_0\left(V_0 - V_{k-k_F}\right)\right]^2 \frac{(k-k_F)^4}{m^3 v_F^6}, \tag{58}$$

where V_q is the Fourier transform of $V(r)$. We will be particularly interested below in the case of power-law decaying interactions

$$V(r) = \frac{1}{ml_0^{2-\alpha}}\frac{1}{r^\alpha}, \tag{59}$$

for which $V_0 - V_q \propto q^{\alpha-1}$. Here, $1 \leqslant \alpha < 3$, and the length l_0 parametrizing the strength of the interaction is the Bohr radius for the potential $V(r)$. Estimating now the relevant momentum k as $k - k_F \sim \Delta\rho$, we find the inelastic decay rate[32]

$$\frac{1}{\tau_p} \sim \frac{1}{m^7 v_F^6 l_0^8}(l_0\rho_\infty)^{2\alpha-2}(l_0\Delta\rho)^{2+2\alpha}. \tag{60}$$

If the interaction falls off faster than $1/r^3$, one has $V_0 - V_q \propto q^2$; the corresponding result can be obtained by setting $\alpha = 3$ in Eq. (60). On the other hand, the characteristic time scale for the density ripples is the shock time $t_c \sim m\Delta x/\Delta\rho$. Assuming moderate interaction strength $l_0 \sim 1/\rho_\infty$, we find

$$\frac{t_c}{\tau_p} \sim N\left(\frac{\Delta\rho}{\rho_\infty}\right)^{2\alpha}. \tag{61}$$

We see that in the limit of small $\Delta\rho/\rho_\infty \ll 1$ the characteristic time τ_p of inelastic decay given by Eq. (60) is much larger than the shock time t_c. In other words, the relaxation effects remain negligibly small at times much larger than t_c. In view of this, in the rest of the paper we neglect the influence of inelastic relaxation on the dynamics and focus on other interaction-induced effects that strongly affect the development of density oscillations.

A. Finite-range interaction

Let us first briefly discuss the influence of finite-range interaction on the dynamics of fermions. We parametrize the interaction potential at low momenta by the scattering length l_0 and the effective interaction radius $l_{\rm int}$:

$$V_q = \frac{1}{ml_0}\left(1 - q^2 l_{\rm int}^2 + \cdots\right) \simeq \frac{1}{ml_0} - \frac{q^2 l_1}{m}, \tag{62}$$

where $l_1 = l_{\rm int}^2/l_0$. Correspondingly, the interaction-induced correction to the Hamiltonian takes the form

$$H_{\rm int} = \frac{1}{2}\int dx\left[\frac{\rho^2}{l_0} - l_1\left(\partial_x\rho\right)^2\right]. \tag{63}$$

Within the hydrodynamic description, the fermionic mass m manifests itself only via the time scale t_c and we have set m to unity (cf. the case of free fermions, Sec. II). We see that the zero-momentum component of interaction gives rise to an additional ρ^2 term in the Hamiltonian. The only effect of this correction is the renormalization of Fermi velocity. The q^2 part of the potential $V(q)$ renormalizes the ρ_x^2 term in the free Hamiltonian. The resulting term may compete with the last term (the one containing the Hilbert transform) of Eq. (57) in governing the dispersive regularization of the shock dynamics. If the interaction range is not too long, $l_1 \ll 1/\Delta\rho$ (this is in particular the case for a short-range interaction with $l_1 \lesssim \lambda_F$), the interaction-induced ρ_x^2 term can be discarded, and the dynamics will be the same as in the free-fermion case. In the opposite limit of a very-long-range interaction $l_1 \gg 1/\Delta\rho$, it is the the interaction-induced term that will control the dispersive regularization. Consequently, the period of oscillations will not be given any more by the free-fermion result (56) but rather will have a form of Eq. (33) with λ_F replaced by l_1, which yields

$$\delta x \sim \sqrt{l_1/\Delta\rho} \gg 1/\Delta\rho. \tag{64}$$

Corresponding equations and their solutions are discussed in Appendix A; the only difference is that the dispersive term is now enhanced by a factor $\sim\rho_\infty l_1$. Similarly to what we will see below for power-law interactions (Secs. IV B and IV C), the character of resulting oscillations will now depend on the sign of the initial pulse. Let us assume that the interaction is repulsive. Then, for an initial density dip the oscillation will have a shape similar to those of free fermions [but with a larger period according to Eq. (64)]. On the other hand, for an initial hump, the perturbation will decompose in a sequence of well-separated solitons (cf. Fig. 9). The particle number q carried by each soliton is obtained from Eq. (A18) by a replacement $1/\rho_\infty \to l_1$, which results in $q \sim \sqrt{l_1\Delta_\rho} \gg 1$.

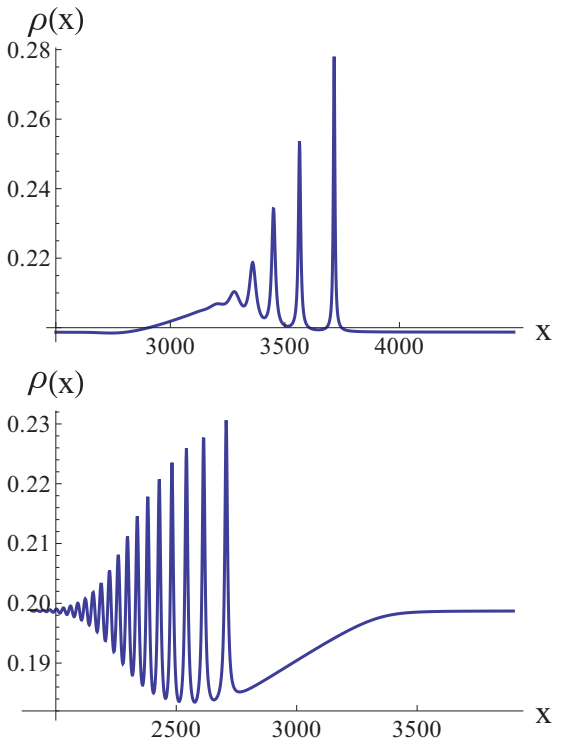

FIG. 9. (Color online) Density profile for the Calogero model with strong repulsive interaction after the shock $t \simeq 5t_c$ as obtained from numerical solution of hydrodynamic equations corresponding to action (69). Initial perturbation was a density hump (top panel) and density dip (bottom panel). In the case of a density hump, the initial Gaussian density perturbation decays into solitons carrying exactly one electron each. On the other hand, for a downward density pulse in the initial state, nearly sinusoidal oscillations develop in the shock region, so that the density evolution is similar to that of free fermions. Note that for a density dip, the shock occurs on the rear side of the pulse.

B. Calogero model

The Calogero-Sutherland (CS) model[33,34] is a remarkable example of the quantum integrable model. It appears in various branches of physics, such as spin chains, disordered metals, and fractional quantum Hall edges.[12,35–38]

In the CS model, the particles interact via an inverse-square potential

$$V(x) = \frac{\lambda(\lambda-1)}{mx^2}. \tag{65}$$

Here, λ is the dimensionless interaction strength and m is particle mass. We will confine ourselves to the case of strong repulsion $\lambda \gg 1$.

Being interested in the hydrodynamic description of the CS model,[11,39–42] we have to rewrite the CS Hamiltonian in terms of the particle density. While the free part of the Hamiltonian

after bosonization turns into the cubic Hamiltonian (21), we need also a regularized expression for the interaction term

$$H_{\rm int} = \frac{1}{2}\int dx\, dx' V(x-x')\rho(x)\rho(x'). \tag{66}$$

The necessity of the regularization arises due to singularity of $V(x)$ at $x = 0$ and the corresponding ultraviolet divergence of the interaction at zero momentum. Taking the inverse particle density as the natural ultraviolet cut-off in the problem, we can rewrite the interaction term as

$$H_{\rm int} \sim \lambda(\lambda-1)\int dx\, \rho^3 - \frac{\lambda(\lambda-1)}{2}\int dx\, \rho\widehat{A}_2\rho\,. \tag{67}$$

The operator $\widehat{A}_2$ was defined in Eq. (35). The precise coefficient in front of the cubic term entering $H_{\rm int}$ is out of control within this estimate. Also, terms with higher gradients of the density may appear upon accurate regularization of the model. A more rigorous treatment of the CS model[29,39,43] leads to a slight modification of Eq. (67) and results in

$$H = \int dx \left[\frac{\rho v^2}{2} + \frac{\pi^2\lambda^2\rho^3}{6} - \frac{\lambda(\lambda-1)}{2}\rho\widehat{A}_2\rho + \frac{(\lambda-1)^2}{8}\frac{\rho_x^2}{\rho}\right]. \tag{68}$$

At $\lambda = 1$, this Hamiltonian reduces to the free Hamiltonian (21).

The characteristic feature of the Calogero model is the scaling of the interaction with distance which coincides exactly with that of the kinetic energy. At large coupling constant $\lambda \gg 1$, the potential energy dominates over the kinetic energy at all scales and drives the model towards the semiclassical limit. Indeed, rescaling by λ the density and the space-time coordinates and switching to Lagrangian formalism, one finds the action corresponding to Eq. (68):

$$S = \lambda\int dx\, dt\left[\frac{1}{2}\frac{\phi_t^2}{\phi_x} - \frac{1}{8}\frac{\phi_{xx}^2}{\phi_x} - \frac{\pi^2}{6}\phi_x^3 + \frac{1}{2}\phi_x\widehat{A}_2\phi_x\right]. \tag{69}$$

Here, $\partial_x\phi = \rho$. The large factor λ in Eq. (69) justifies now the semiclassical approach.

Note that the Lagrangian in Eq. (69) is precisely the "hole" (not particle!) Lagrangian L_h we encountered in our discussion of loop corrections to hydrodynamics of free fermions [see Eq. (37) of Sec. III C]. The corresponding equations of motion are the Euler equations (31) with the enthalpy given by Eq. (39) except for additional minus sign in front of the nonlocal term.

This change of sign has a dramatic effect on the density evolution in the system after the shock, as illustrated in Fig. 9 (top panel) where we plot the fermionic density at $t \approx 5t_c$ for the same initial density hump as was used previously. The density evolution was obtained via the numerical solution of hydrodynamic equations corresponding to action (69). In the shock region, instead of the dispersive wave seen in Fig. 8, one observes the formation of a solitonic train. Thus, at late stages of the evolution, the initial hump decays into well-separated solitons. Each of the solitons carries exactly one particle. The quantization of solitonic charge, which is equal to unity, is a distinct feature of the strongly repulsive Calogero model.

The solitonic train in the shock region can be studied analytically via the solution of modulation equations discussed previously in Sec. III C. One finds (see Appendix C for details) that close to the front edge of the train, the height and width of the solitons (which are of Lorentzian shape) are given by

$$\delta\rho = 2\Delta\rho\,, \quad \delta x = \frac{1}{2\pi\Delta\rho}\,. \tag{70}$$

The density evolution is very much different (and much more similar to that of free fermions) for the case of an initial density dip. The corresponding data are shown in the bottom panel of Fig. 9; they are fully analogous to the previous results of Fig. 8. (Note that for a density dip the shock occurs on the rear side of the pulse.) We see that a nearly sinusoidal dispersive wave is formed in the shock region.

Such a dramatic difference in the behavior of particlelike and holelike pulses has a simple qualitative explanation. A soliton can be formed when the effects of nonlinearity and dispersion on the velocity counteract; their balance yields a soliton that moves preserving its shape. In the case of the Lagrangian (69) [which is equivalent, up to an overall factor λ, to L_h of Eq. (37)], the dispersive term reduces the velocity [see Eq. (36)], with the lower sign corresponding to L_h. Therefore, solitons can form if the nonlinear term will enhance the velocity. This is the case when $\Delta\rho$ is positive, i.e., for a density hump.

C. Coulomb and other slowly decaying interactions

Let us now turn to interactions decaying slower than the inverse distance squared (for definiteness, we will assume a repulsive interaction),

$$V_\alpha(r) = \frac{1}{ml_0^{2-\alpha}}\frac{1}{r^\alpha}\,, \tag{71}$$

with an exponent α satisfying $1 \leqslant \alpha < 2$. The case $\alpha = 1$ corresponds to the Coulomb interaction and is the most relevant from the experimental point view. Throughout this section, we will assume the interaction to be weak in the sense that the parameter $r_s = \lambda_F/l_0$ is small, $r_s \ll 1$. (There is no problem in analyzing the strong interaction regime $r_s \gtrsim 1$ in a similar way, and we expect a qualitatively similar behavior.) For $\alpha = 1$ we will also assume that the Coulomb interaction is screened at a sufficiently large distance $d \gg l_0$.

The reasoning of the previous section which led us to Eq. (67) is easy to generalize for the present case with the result

$$H_{{\rm int},\alpha} \simeq \frac{1}{l_0^{2-\alpha}}\int dx\left(\rho^{\alpha+1} - \frac{1}{2}\rho\widehat{A}_\alpha\rho\right), \tag{72}$$

$$A_\alpha(q) = -2\Gamma[1-\alpha]\sin\frac{\pi\alpha}{2}|q|^{\alpha-1}\,, \quad \alpha > 1 \tag{73}$$

$$A_1(q) = \ln qd\,, \quad qd \gg 1\,. \tag{74}$$

In the Coulomb case, the $\rho^{\alpha+1}$ term in $H_{{\rm int},\alpha}$ should be replaced by $(\rho^2\ln d\rho)/l_0$. For $\alpha > 1$, the precise numerical coefficient in front of the $\rho^{\alpha+1}$ term can not be found within this reasoning. On the other hand, this term is small in parameter r_s compared to the cubic term in the Hamiltonian of free fermions which provides the dominant nonlinearity. The only effect of the nonlinear contribution $H_{\rm int}$ is a renormalization of Fermi

velocity (small at $r_s \ll 1$) and we can omit it. Combining the free bosonized Hamiltonian with the relevant (dispersive) part of the interaction correction, we find

$$H = \int dx \left[\frac{\rho v^2}{2} + \frac{\pi^2 \rho^3}{6} - \frac{1}{2} \rho \widehat{A}_\alpha \rho \right]. \tag{75}$$

As we have found previously, the loop contribution to the equations of motion can be modeled by a correction to the Hamiltonian of the form

$$\delta H_{\text{loop}} \simeq \int dx\, \rho \widehat{A}_2 \rho\,. \tag{76}$$

Comparing the interaction-induced dispersive contribution [last term in Eq. (75)] to Eq. (76), we see that the interaction controls the dispersive effects at scales larger than l_0.

The characteristic scale developed by the density perturbation after the shock results from the tradeoff between nonlinearity and dispersion. For $\alpha > 1$, the corresponding estimate yields the scale

$$\delta x \sim l_0 \frac{1}{(l_0 \Delta\rho)^\beta}\,, \quad \beta = \frac{1}{\alpha - 1}. \tag{77}$$

We see that δx is indeed much larger than l_0 provided that

$$l_0\, \Delta\rho \ll 1\,. \tag{78}$$

In the Coulomb case under the same assumptions we get

$$\delta x \sim d \gg l_0. \tag{79}$$

Thus, under the assumption (78) the physics of density oscillations is indeed dominated by scales much larger than l_0, so that the neglect of loop corrections is justified.

Experience gained in the analysis of the Calogero model and free fermions allows us to predict qualitative features of the density evolution, most prominently, its dependence on the sign of the density perturbation and the sign of the interaction. Specifically, we expect that for repulsive interaction and

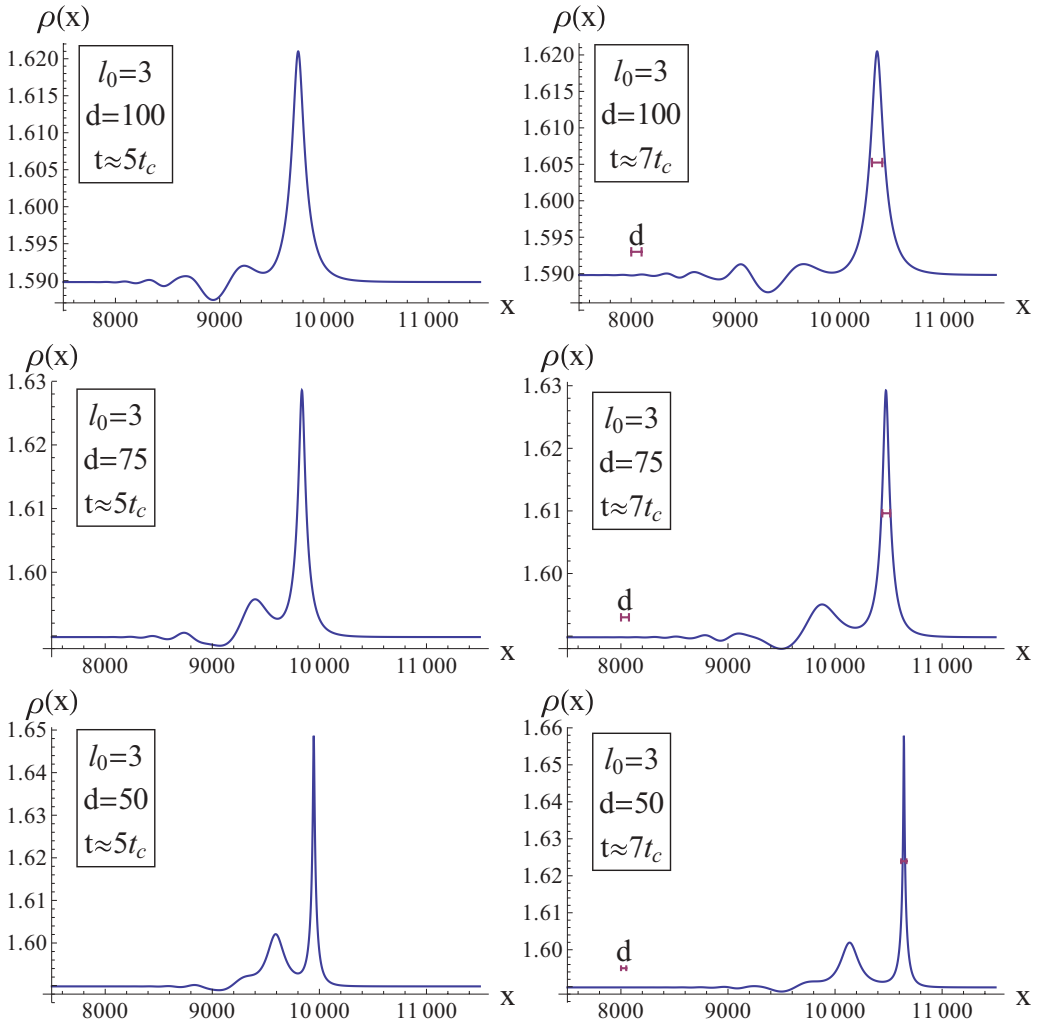

FIG. 10. (Color online) Density profile after the shock for the case of Coulomb interaction. The initial density perturbation is positive and coincides with the one used in Sec. II (up to the constant equilibrium density ρ_∞). The Bohr radius l_0, the screening length d, and the snapshot time t are indicated in each graph. For convenience of presentation, a constant coordinate shift has been made: $x \to x - 20\,000$ for the left ($5t_c$) plots and $x \to x - 30\,000$ for the right ($7t_c$) plots. For the upper two and the middle two graphs, the half-maximum width of the main peak is approximately given by d, as shown in the right plots. For the two bottom graphs, the width is smaller than d by a factor $\approx$1.5. This deviation from scaling with decreasing d is probably related to the fact that the condition (78) becomes less well satisfied.

positive perturbation a train of solitary waves should emerge in front of the pulse. Each solitary wave is expected to carry $\delta x \Delta\rho \gg 1$ particles. On the other hand, a downward density perturbation (for the same repulsive interaction) will lead to formation of a nearly sinusoidal dispersive wave in the shock region. The change of the sign of interaction will result in the interchange of these two types of behavior.

To support the qualitative analysis presented above, we have performed numerical simulations of the hydrodynamic equations dictated by the Hamiltonian (75). Let us discuss the Coulomb case first. Figure 10 shows the density perturbation for times $t = 5t_c$ and $7t_c$ for electrons interacting via a Coulomb potential. The initial density hump was Gaussian with the same parameters as in the previous sections except for the equilibrium density ρ_∞ which was taken larger to ensure that $l_0 \gtrsim \lambda_F$.[44] Values of the parameters l_0 and d as well as of the time t are indicated in each of the plots. We clearly observe formation of a solitary wave and beginning of the formation of a second one (better pronounced for smaller d). According to the estimates presented above, in the Coulomb case the characteristic scale of the density oscillations emerging after the shock should be given simply by the screening length d. This is indeed confirmed by our numerics. In particular, the half-maximum width of the main peak in the plots with $d = 100$ and 75 is equal to d. The two bottom plots (with the smallest d equal to 50) demonstrate some deviation from this scaling. This is possibly related to the fact that the condition (78) becomes less well satisfied in view of increasing amplitude $\Delta\rho$ of the peak.

Figure 11 illustrates the change of the density behavior upon the change in of the sign of the density perturbation. As expected, for negative $\Delta\rho$ we observe onset of nearly sinusoidal oscillations with a period $\sim d$ in the shock region.

We have also performed numerical study of fermions interacting via the intermediate potential $V_{3/2}(x)$. The results are exemplified in Fig. 12. We observe that the density develops a solitary wave, similarly to the case of Coulomb interaction Fig. 10. The scaling of the width of the soliton

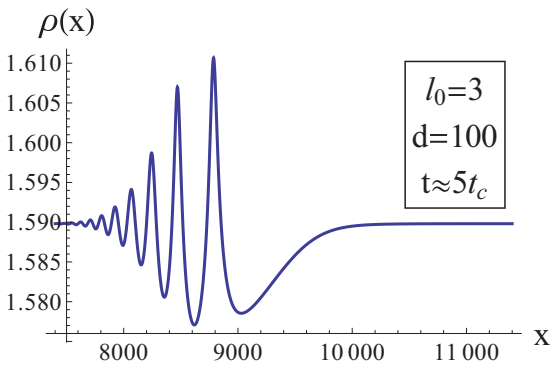

FIG. 11. (Color online) Density profile after the shock for the case of Coulomb interaction. The initial density perturbation differs from the Gaussian pulse of Sec. II by the change of sign. The legend indicates the Bohr radius l_0 and the screening length d. For convenience of presentation, a constant coordinate shift $x \to x - 30\,000$ has been made. In contrast to the case of a positive (upward) density pulse (Fig. 10), a nearly sinusoidal oscillatory behavior is observed in the shock region.

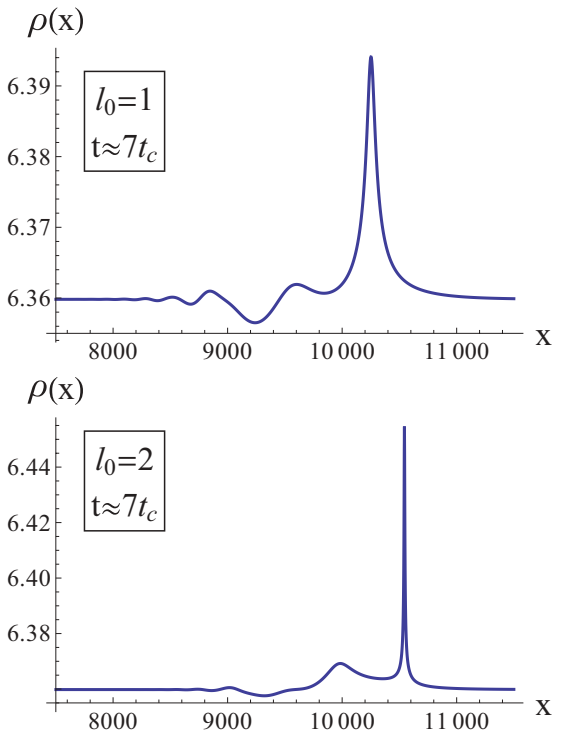

FIG. 12. (Color online) Density profile after the shock (time $t \simeq 7t_c$) for electrons interacting via the $r^{-3/2}$ potential. The initial density perturbation is positive and coincides with the one used in Sec. II (up to the equilibrium density ρ_∞). The Bohr radius l_0 is indicated in the plots. For convenience of presentation, a constant coordinate shift $x \to x - 120\,000$ has been made.

agrees well with our above estimate of the characteristic scale for $\alpha = \frac{3}{2}$,

$$\delta x \sim \frac{l_0}{(l_0\Delta\rho)^2}, \tag{80}$$

if we use for $\Delta\rho$ the actual amplitude of the peak. (While in the Calogero $1/r^2$ case the soliton amplitude $\Delta\rho$ is determined by that of the initial pulse, this is no more true for $\alpha < 2$.) Note that the parameter $l_0\Delta\rho$ remains sufficiently small ($\simeq 0.04$ for the upper plot and 0.2 for the lower plot), so that the neglect of loop corrections is reasonably well justified.

The analytical arguments and numerical data presented above unambiguously show that a sufficiently strong and sufficiently long-ranged interaction dominates over quantum corrections in controlling the dispersive effects. In this limit, the Hamiltonian (75) and corresponding hydrodynamic equations provide a controlled description of the nonequilibrium dynamics in a quantum many-body system.

V. SUMMARY AND OUTLOOK

In this article, we have explored the evolution of a density pulse in a 1D fermionic fluid. Our focus was on the regime of a wave "overturn" (population inversion) that is induced by spectral curvature. We showed that beyond the corresponding time, the density profile develops strong oscillations with a period much larger than the Fermi wavelength and performed a detailed analysis of these oscillations. We have considered

the case of free fermions as well as various interacting models, including a finite-range interaction, CS model, generic power-law interaction, and screened Coulomb interaction. Our key results can be summarized as follows:

(1) For the case of free fermions, we have studied the problem by means of direct quantum simulations. Further, we have obtained an analytical solution using the phase-space representation and the Wigner function. The Wigner function of the initial state exhibits oscillations in the phase space (as a function of the momentum). When the initial perturbation is allowed to propagate (i.e., after the quench), the curvature of single-particle spectrum leads to the formation of inverse population of electrons at times $t > t_c$. In this regime, the oscillations of Wigner function in phase space induce real-space density oscillations, with each "ripple" containing a fraction of an electron. The characteristic period of these oscillations is controlled by the amplitude $\Delta\rho$ of perturbation and is independent of the equilibrium density ρ_∞ (or, equivalently, of the wavelength λ_F).

(2) We have also addressed the free-fermion problem using a hydrodynamic approach. The semiclassic equation of motion leads to formation of a shock in the regime where the inverse population of fermions in the momentum space is generated. This shock is regularized by gradient corrections to the Hamiltonian and by quantum fluctuations. We show that for free fermions the latter effect is more important. We model the quantum correction by including in the theory a dispersive term corresponding to a particle or hole branch of the fermionic spectrum, depending on the sign of the initial perturbation. This yields two different hydrodynamic theories (with a difference in the sign of the dispersive term) for upward and downward density pulses.

We show that this approach correctly captures the period of shock-induced density oscillation, but overestimates their amplitude. In the hydrodynamic language, the formation of oscillations is caused by an interplay of the nonlinearity and the dispersion (dominated, in the case of free fermions, by quantum corrections). For free fermions, both nonlinearity and dispersion are entirely due to spectral curvature.

(3) The electron interaction leads to additional dispersive terms in the hydrodynamic equations. For interaction that decays with the distance r slower than $1/r^2$, such terms dominate the long-distance (small-momentum) behavior, and quantum correction can be neglected. In this case, the applicability of semiclassical hydrodynamic equations becomes fully justified. The case of CS model ($1/r^2$ interaction) is marginal; the interaction-induced dispersive term is dominant (and thus the semiclassical hydrodynamic approach is fully controlled) if the interaction is strong, $\lambda \gg 1$.

For the case of a finite-range interaction, the dominant dispersive term is provided by the interaction only if the interaction radius is very big; otherwise, the free-fermion results apply.

(4) In the situations when the interaction controls the dispersive effects (and thus the semiclassical hydrodynamic approach is fully under control), the impact of interaction depends on its sign and the sign of the density perturbation. Specifically, for a repulsive interaction and a density dip (as well as for an attractive interaction and a density hump), we observe formation of nearly sinusoidal oscillatory structure similar to the free-fermions case. Quantitative characteristics of the oscillations (wavelength and a number of particles in each "ripple") are, however, in general parametrically different compared to the free-fermion model.

On the other hand, for a repulsive interaction and a density hump (as well as for an attracting interaction and a density dip), the interaction leads to the formation of a train of solitary waves. In general, the charge (particle number) carried by each soliton is nonuniversal (depends on the type and the strength of the interaction, and on the amplitude of the perturbation). A notable exception is the CS model with $\lambda \gg 1$, when the solitons carry a unit charge.

We hope that our predictions can be verified experimentally. There are a number of electronic realizations of 1D fermionic systems, including carbon nanotubes, semiconductor and metallic nanowires, as well as quantum Hall and topological insulator (quantum spin Hall) edges. For these electronic liquids, a model with Coulomb interaction is expected to be applicable (except if special efforts are made to strongly screen it). An alternative physical realization is provided by systems of cold fermionic atoms. This is probably the most natural experimental realization of the models of free fermions and of finite-range interaction.

Before closing, we list some of directions of further theoretical research opened by this paper; a work in some of these directions is currently underway.

(1) An interesting question is whether it is possible to formulate a more general classical hydrodynamic theory for free fermions that would controllably capture evolution of a generic density perturbation, including both upward and downward density pulses. Such a theory can be useful from the fundamental point of view, as well as for the problem in which quantum corrections and interaction effects are comparable.

(2) For models with power-law interaction other than the CS model (including the experimentally most relevant case of the Coulomb interaction), it is important to complete analytical investigation of the emerging oscillations and solitary waves and to explore the scattering of excitations in these theories.

(3) An important task is to perform *ab initio* calculations for many-body quantum interacting system. The results should allow one to verify our above predictions (obtained in the framework of the hydrodynamic theory) and to explore the interplay of quantum corrections and interaction (e.g., in the model with a finite-range interaction).

(4) Our results on evolution of a density perturbation should be also relevant to strongly repulsive 1D bosonic problems, in particular, in view of the equivalence between the Tonks-Girardeau gas and free fermions. It would be very interesting to study the crossover from the quasicondensate regime characteristic for weakly interacting bosons[17,45] to the Fermi-type behavior for strong repulsion. On the experimental side, such a setup can be realized in the framework of cold bosonic atoms.

ACKNOWLEDGMENTS

We thank M. Hoefer for sharing his expertise on numerical analysis of hydrodynamic equations, I. Gornyi for useful discussions and collaboration on a related project,[46] and L. Glazman for useful discussions. While preparing this

work for publication, we learned about a related activity on the free-fermion problem.[47] Financial support by Alexander von Humboldt Foundation (I.V.P.), Israeli Science Foundation Grant No. 819/10 (D.B.G.), German Israeli Foundation, and DFG priority programs SPP1243 and SPP1285 is gratefully acknowledged.

APPENDIX A: HYDRODYNAMICS DEFINED BY EQS. (31) AND (32): SOLITONS AND PERIODIC SOLUTIONS

In this Appendix, we analyze properties of the classical hydrodynamics defined by Eqs. (31) and (32). Such a theory arises if we take into account dispersive terms generated by phenomenological Haldane's formalism (see Sec. III A), but neglect the quantum loop correction.

As explained in the main text, this turns out to be *not* a correct description of free fermions (since the loop corrections generate parametrically more important dispersive terms). Nevertheless, the analysis of this theory is quite illuminating, and we present it in this appendix. Furthermore, such a theory arises in a fully controllable way in a model of finite-range interaction with a sufficiently large interaction radius (see Sec. IV A).

Let us focus on traveling wave excitations

$$\rho(x,t) = \rho(x - Vt), \tag{A1}$$

$$v(x,t) = v(x - Vt). \tag{A2}$$

Substituting Eq. (A1) into Eq. (31), one finds

$$-V\partial_x\rho + \partial_x(\rho v) = 0, \tag{A3}$$

$$\partial_x\left(-Vv + \tfrac{1}{2}v^2 + w\right) = 0. \tag{A4}$$

We now analyze some simple excitations described by Eqs. (A3) and (A4).

1. Single soliton

We start with a solitonic wave. In this case, the excitation of the density and velocity fields is confined to a finite region in space, and the continuity equation (A3) yields

$$v = V\frac{\rho - \rho_\infty}{\rho}. \tag{A5}$$

Substituting Eq. (A5) into Euler equation (A4), one obtains

$$\rho_x\left(\frac{V^2}{2}\frac{\rho_\infty^2 - \rho^2}{\rho^2} + \frac{\pi^2\rho^2}{2} - \frac{\pi^2\rho_\infty^2}{2}\right) = \frac{1}{8}\partial_x\left(\frac{\rho_x^2}{\rho}\right). \tag{A6}$$

Since both sides of the equation are full derivative with respect to x, the order of this equation can be easily reduced, yielding

$$\rho_x^2 = 4\left[-V^2\rho_\infty^2 - V^2\rho^2 + \frac{\pi^2}{3}\rho^4 - \pi^2\rho_\infty^2\rho^2 + 4E\rho\right]. \tag{A7}$$

Here, $E = \rho_\infty V^2/2 + \pi^2\rho_\infty^3/6$ is a constant of integration. Defining $\xi = \rho - \rho_\infty$, one obtains

$$\int \frac{d\xi}{\xi\sqrt{a + b\xi + c\xi^2}} = 2x, \tag{A8}$$

where $a = \pi^2\rho_\infty^2 - V^2$, $b = 4\pi^2\rho_\infty/3$, $c = \pi^2/3$. Performing the integral over ξ, we find the solitonic solution

$$\xi(x) = \frac{4az}{(z-b)^2 - 4ac}, \tag{A9}$$

$$z = \frac{2a + b\xi_0}{\xi_0}e^{-2\sqrt{a}|x|}, \tag{A10}$$

where $\xi_0 < 0$ is the largest (smallest by absolute value) root of $a + b\xi + c\xi^2$. We note that solitons propagate with the velocity smaller than the velocity of sound ($V < \pi\rho_\infty$), i.e., is a holelike excitation from the fermionic point of view. The charge of a soliton

$$q = \frac{\sqrt{3}}{2\pi}\ln\frac{2 - \sqrt{3(1-\widetilde{V}^2)}}{2 + \sqrt{3(1-\widetilde{V}^2)}}, \quad \widetilde{V} = \frac{V}{\pi\rho_\infty} \tag{A11}$$

is less than unity and is not quantized.

2. Periodic wave

Periodic solutions of Eqs. (A3) and (A4) can be conveniently parametrized by $\lambda_4 > \lambda_3 > \lambda_2 > \lambda_1$:

$$(\partial_x\rho)^2 = \frac{4\pi^2}{3}(\rho - \lambda_1)(\rho - \lambda_2)(\rho - \lambda_3)(\rho - \lambda_4), \tag{A12}$$

where parameters λ satisfy the constraint $\lambda_1 + \lambda_2 + \lambda_3 + \lambda_4 = 0$, and are related to the velocity of the wave according to

$$V^2 = \frac{\pi^2}{3}\left(\lambda_2^2 + \lambda_3^2 + \lambda_4^2 + \lambda_2\lambda_3 + \lambda_2\lambda_4 + \lambda_3\lambda_4\right). \tag{A13}$$

The Euler equation (A4) can thus be rewritten as

$$\frac{d\rho}{\sqrt{(\lambda_4 - \rho)(\lambda_3 - \rho)(\rho - \lambda_2)(\rho - \lambda_1)}} = \sqrt{\frac{4\pi^2}{3}}dx. \tag{A14}$$

Integrating this equation, we find

$$\rho(x) = \frac{\lambda_1(\lambda_4 - \lambda_2)[1 - \mathrm{dn}^2(y;k)] - \lambda_2(\lambda_4 - \lambda_1)}{(\lambda_4 - \lambda_2)[1 - \mathrm{dn}^2(y;k)] - (\lambda_4 - \lambda_1)}. \tag{A15}$$

Here, $\mathrm{dn}(y;k)$ is a Jacobi elliptic function $y = x\sqrt{(\lambda_4 - \lambda_2)(\lambda_3 - \lambda_1)\pi^2/3}$, and the elliptic modulus k is given by

$$k^2 = \frac{(\lambda_3 - \lambda_2)(\lambda_4 - \lambda_1)}{(\lambda_3 - \lambda_1)(\lambda_4 - \lambda_2)}. \tag{A16}$$

The density oscillates within the interval $\lambda_2 \leqslant \rho \leqslant \lambda_3$. The limit $\lambda_1 < \lambda_2 < \lambda_3 \to \lambda_4$ corresponds to trains of well-separated dips (which are nothing but solitons considered above), where the size of each dip d is much shorter then the distance between the neighboring dips L. In this regime, the width of the dip can be related to the density amplitude $\delta\rho$ as

$$d \sim \frac{1}{\sqrt{\delta\rho\,\rho_\infty}}. \tag{A17}$$

The number of particles carried by a dip can be estimated as

$$q = d\delta\rho \sim \sqrt{\delta\rho/\rho_\infty} \leqslant 1. \tag{A18}$$

The limit $\lambda_1 < \lambda_2 \to \lambda_3 < \lambda_4$ describes a small-amplitude periodic wave. The amplitude of the wave is $\lambda_3 - \lambda_2$, and its wavelength is $L = \sqrt{3/4\pi^2(\lambda_4 - \lambda_3)(\lambda_2 - \lambda_1)}$. Thus, the

number of electrons carried by each "ripple" (period) of the wave is

$$q \sim \frac{\lambda_3 - \lambda_2}{\sqrt{(\lambda_4 - \lambda_3)(\lambda_2 - \lambda_1)}} \ll \sqrt{\frac{\delta\rho}{\rho_\infty}} \ll 1. \quad \text{(A19)}$$

It is worth mentioning that the theory considered in this appendix bears a close connection with the KdV equation of the classical hydrodynamics. This is because the regularizing term in the hydrodynamic equations has a similar (third-derivative) structure in both cases.

APPENDIX B: MODULATION EQUATIONS FOR HYDRODYNAMICS DEFINED BY EQS. (31) AND (39)

In this section, we address the issue of modulation equations for the hydrodynamic system (31) and (39). Within the framework of Whitman modulation theory, one promotes the single-phase (periodic) wave (40) to an ansatz

$$\phi = \widetilde{\theta}(x,t) + \Phi[\theta(x,t),x,t] \quad \text{(B1)}$$

and identifies the parameters of the single-phase wave with the derivatives of the phases θ and $\widetilde{\theta}$:

$$\rho_0 = \partial_x \widetilde{\theta}\,, \quad \gamma = -\partial_t \widetilde{\theta}, \quad \text{(B2)}$$

$$k = \partial_x \theta\,, \quad \omega = -\partial_t \theta. \quad \text{(B3)}$$

Obviously, parameters defined in this way satisfy the continuity equations

$$\partial_t \rho_0 + \partial_x \gamma = 0\,, \quad \partial_t k + \partial_x \omega = 0. \quad \text{(B4)}$$

To derive the modulation equations, we substitute the single-phase waves (40), (41), (42), and (43) into the Lagrangian L_p, neglect derivatives of the modulation parameters, and average the result over a period of oscillations. We get

$$\langle L_p \rangle = -\frac{1}{6}\pi^2\rho_1^3 + \frac{\gamma^2}{2\rho_1} + \frac{\gamma\omega}{2\pi\rho_1} + \frac{\omega^2}{8\pi^2\rho_1} + \frac{k^3}{48\pi} - \frac{\omega^2}{4\pi k} + \sigma\left(-\frac{\rho_1\omega}{2} + \frac{\gamma k}{2} + \frac{k\omega}{4\pi}\right). \quad \text{(B5)}$$

Here, $\sigma = \mathrm{sign}\,(k\gamma - \omega\rho_0)$ and ρ_1 is given by Eq. (43). We now vary the averaged Lagrangian (B5) with respect to phases $\widetilde{\theta}$ and θ, keeping in mind the relations (B2) and (B3). This yields

$$\partial_x \frac{\partial\langle L_p\rangle}{\partial k} + \partial_t \frac{\partial\langle L_p\rangle}{\partial\omega} = 0. \quad \text{(B6)}$$

$$\partial_x \frac{\partial\langle L_p\rangle}{\partial \rho_0} + \partial_t \frac{\partial\langle L_p\rangle}{\partial\gamma} = 0. \quad \text{(B7)}$$

These two equations, together with the continuity equations, constitute four equations for the four unknown parameters. Writing them explicitly and performing a change of variables according to Eqs. (47)–(50), we arrive at Eq. (46).

Figure 13 demonstrates the density in the shock region predicted by modulation theory together with the result of numerical simulations. We observe a perfect agreement between the analytical and numerical results.

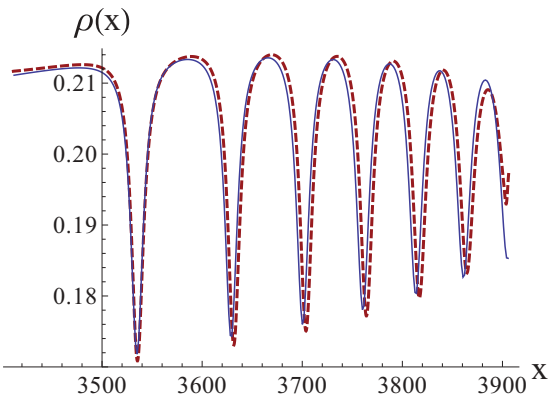

FIG. 13. (Color online) Comparison of predictions of the modulation theory (dashed line) and numerical simulations (full line) for the hydrodynamic theory (31) and (39). A perfect agreement between the analytic and numerical results is observed.

APPENDIX C: MODULATION THEORY AND SOLITON TRAINS IN THE CALOGERO MODEL

In Appendix B, we have discussed in detail the modulation theory of hydrodynamic equations (31) and (39) generated by the "particle" Lagrangian L_p [Eq. (37)]. Let us now briefly address the modulation equations for the theory defined by the "hole" Lagrangian L_h and their solution for the upward density perturbation in the initial state. This issue is relevant for the description of the solitonic train emerging from the positive density perturbation in the repulsive Calogero fluid (see Sec. IV B).

The starting point for the modulation theory is a single-phase periodic wave. Its form can be obtained from Eqs. (42)–(44) via the replacement $k \to -k$ and $\omega \to -\omega$. The modulation equations can now be derived exactly in the same way as in Appendix B. The result reads as

$$k = u_3 - u_2, \quad \text{(C1)}$$

$$\omega = \frac{1}{2}(u_3^2 - u_2^2), \quad \text{(C2)}$$

$$\rho_0 = \frac{-u_0 + u_1 - u_2 + u_3}{2\pi}, \quad \text{(C3)}$$

$$\gamma = \frac{-u_0^2 + u_1^2 - u_2^2 + u_3^2}{4\pi}, \quad \text{(C4)}$$

with the Riemann invariants u_i satisfying

$$\partial_t u_i + u_i \partial_x u_i = 0. \quad \text{(C5)}$$

Finally, applying the boundary conditions (51) and (52) at the edges of shock region, one finds the Riemann invariants in term of the branches of Fermi momentum $p_F^{(i)}$ (see Fig. 2):

$$u_i = p_F^{(i)}, \quad i = 1,2,3 \quad \text{(C6)}$$

$$u_0 = -p_\infty. \quad \text{(C7)}$$

Here, we have chosen labeling of Riemann invariants u_i such that they exactly correspond [see Eq. (C6)] to our notations for Fermi-momentum branches, as was also the case for the Lagrangian L_p [Eq. (53)]. Note that the relations between the

parameters k, ω, ρ_0, γ and the Riemann invariants differ in the two cases by cyclic permutation of u_1, u_2, and u_3 [cf. Eqs. (47)–(50) and Eqs. (C1)–(C4)].

Contrary to the case of "particle" Lagrangian L_p considered in the previous section, Eqs. (C1)–(C4) predict that the wave vector k vanishes at the leading edge x_l and the density perturbation decays into Lorentzian-shaped solitons

$$\rho(x,t) = \rho_\infty + \frac{1}{\pi}\frac{A}{A^2 + (x - Vt)^2}, \tag{C8}$$

$$A = \frac{p_F^{(1)} + p_\infty}{2\left(p_F^{(2)} + p_\infty\right)\left(p_F^{(3)} - p_F^{(1)}\right)}, \tag{C9}$$

$$V = \frac{p_F^{(3)} + p_F^{(2)}}{2}. \tag{C10}$$

In the limit $\Delta\rho \ll \rho_\infty$, this simplifies to

$$\rho(x,t) = \rho_\infty + \frac{2\Delta\rho}{1 + 4\pi^2\Delta\rho^2(x - V_F t)^2}. \tag{C11}$$

[1] M. Stone, *Bosonization* (World Scientific, Singapore, 1994).
[2] J. von Delft and H. Schoeller, Ann. Phys. (NY) **7**, 225 (1998).
[3] A. O. Gogolin, A. A. Nersesyan, and A. M. Tsvelik, *Bosonization in Strongly Correlated Systems* (Cambridge University Press, Cambridge, UK, 1998).
[4] T. Giamarchi, *Quantum Physics in One Dimension* (Clarendon Press, Oxford, 2004).
[5] D. L. Maslov, in *Nanophysics: Coherence and Transport*, edited by H. Bouchiat, Y. Gefen, G. Montambaux, and J. Dalibard (Elsevier, Amsterdam, 2005), p.1.
[6] V. V. Deshpande, M. Bockrath, L. I. Glazman, and A. Yacoby, Nature (London) **464**, 209 (2010).
[7] A. Imambekov and L. I. Glazman, Science **323**, 228 (2009); Phys. Rev. Lett. **102**, 126405 (2009).
[8] A. Imambekov, T. L. Schmidt, and L. I. Glazman, Rev. Mod. Phys. **84**, 1253 (2012).
[9] M. Khodas, M. Pustilnik, A. Kamenev, and L. I. Glazman, Phys. Rev. B **76**, 155402 (2007).
[10] T. Karzig, L. I. Glazman, and F. von Oppen, Phys. Rev. Lett. **105**, 226407 (2010).
[11] E. Bettelheim, A. G. Abanov, and P. Wiegmann, Phys. Rev. Lett. **97**, 246401 (2006).
[12] P. Wiegmann, Phys. Rev. Lett. **108**, 206810 (2012).
[13] G. B. Whitham, *Linear and Nonlinear Waves* (Wiley, New York, 2011).
[14] See Supplemental Material at http://link.aps.org/supplemental/10.1103/PhysRevB.87.045112 for a full movie of density evolution.
[15] In precise terms, the density perturbation was created by a Gaussian potential $U(x) = U_0 e^{-x^2/2\sigma_U^2}$ applied to the unperturbed tight-binding model. The dispersion was chosen to be $\sigma_U = 100$ lattice sites and the amplitude of the potential $U_0 = \mp 0.2$ (for density hump and density dip, respectively). Here, U_0 is measured in units of hopping matrix element.
[16] E. Bettelheim and P. B. Wiegmann, Phys. Rev. B **84**, 085102 (2011).
[17] M. A. Hoefer, M. J. Ablowitz, I. Coddington, E. A. Cornell, P. Engels, and V. Schweikhard, Phys. Rev. A **74**, 023623 (2006).
[18] L. D. Landau, Zh. Eksp. Teor. Fiz. **11**, 592 (1941) [J. Phys. USSR **5**, 71 (1941)].
[19] E. M. Lifshitz and L. P. Pitaevskii, *Statistical Physics, Part 2* (Elsevier, Oxford, 1980).
[20] M. Schick, Phys. Rev. **166**, 404 (1968).
[21] B. Sakita, *Quantum Theory of Many-variable Systems and Fields* (World Scientific, Singapore, 1985).
[22] A. Jevicki and B. Sakita, Nucl. Phys. B **165**, 511 (1980).
[23] F. D. M. Haldane, Phys. Rev. Lett. **47**, 1840 (1981).
[24] At present, the status of Haldane's theory is not fully understood. We believe that it is a phenomenological method that correctly captures the essential features of charge discreetness as well as of single-particle spectrum curvature. It is not clear yet whether it can be accurately derived even for a free-fermion case starting from the first principles. Note that the derivation of quantum Hamiltonian (21) was done using the collective variables approach (Ref. 21). Although the derivation appears solid, it contains a very delicate point (Ref. 46). In deriving Eq. (21), all Fourier modes of the density (ρ_k) were assumed to be independent, $\frac{\partial\rho_q}{\partial\rho_k} = \delta_{k,q}$. While this obviously holds for an infinite number of particles, the limit $N \to \infty$ is delicate. Indeed, for any finite number N, only the lowest N modes of the density can be considered as independent, while all the higher harmonics needs to be expressed in terms of the lower ones. Thus, to treat this limit carefully (Ref. 46), one needs to derive the Hamiltonian for a large but finite number of particles, and only then to take the limit $N \to \infty$.
[25] A. Jevicki, Nucl. Phys. B **376**, 75 (1992).
[26] K. V. Samokhin, J. Phys.: Condens. Matter **10**, L553 (1998).
[27] D. N. Aristov, Phys. Rev. B **76**, 085327 (2007).
[28] While the one-loop analysis of ρ^3 theory performed in Refs. 26 and 27 generates the correct scale for spectral broadening of bosonic excitations, it does not produce sharp boundaries (36) of the spectrum. Within such an approach, the branches (36) should emerge as a result of resummation of the whole perturbative expansion.
[29] D. B. Gutman, Pisma v Zh. Eksp. Teor. Fiz. **86**, 71 (2007) [JETP Lett. **86**, 67 (2007)].
[30] Y. Matsuno, Phys. Rev. E **58**, 7934 (1998).
[31] Y. Matsuno, *Bilinear Transformation Method* (Academic, New York, 1984).
[32] In the estimation of zero-momentum interaction V_0 we have used natural ultraviolet cutoff $1/\rho_\infty$.
[33] F. Calogero, J. Math. Phys. **10**, 2197 (1969).
[34] B. Sutherland, J. Math. Phys. **12**, 246 (1971).
[35] P. J. Forrester, Nucl. Phys. B **388**, 671 (1992); Phys. Lett. A **179**, 127 (1993).
[36] Z. N. C. Ha, Phys. Rev. Lett. **73**, 1574 (1994); *Quantum Many-Body Systems in One Dimension* (World Scientific, Singapore, 1996).
[37] D. M. Gangardt and A. Kamenev, Nucl. Phys. B **610**, 578 (2001).
[38] B. D. Simons, P. A. Lee, and B. L. Altshuler, Phys. Rev. Lett. **70**, 4122 (1993).

[39] A. P. Polychronakos, Phys. Rev. Lett. **74**, 5153 (1995).
[40] H. Awata, Y. Matsuo, S. Odake, and J. Shiraishi, Phys. Lett. B **347**, 49 (1995).
[41] M. Stone, I. Anduaga, and L. Xing, J. Phys. A: Math. Theor. **41**, 275401 (2008).
[42] A. P. Polychronakos, J. Phys. A: Math. Gen. **39**, 12793 (2006).
[43] M. Stone and D. B. Gutman, J. Phys. A: Math. Theor. **41**, 025209 (2008).
[44] We have checked that, as expected, our results do not depend on the density ρ_∞ (up to renormalization of Fermi velocity).
[45] M. Kulkarni and A. G. Abanov, Phys. Rev. A **86**, 033614 (2012).
[46] I. V. Gornyi and D. B. Gutman (unpublished).
[47] E. Bettelheim and L. I. Glazman (unpublished).